PCCP

Accepted Manuscript

ROYAL SOCIETY OF CHEMISTRY

www.rsc.org/pccp

Hybrid QTAIM and Electrostatic Potential-Based Quantum Topology Phase Diagrams for Water Clusters

Anmol Kumar and Shridhar R. Gadre*
Department of Chemistry, Indian Institute of Technology, Kanpur 208016, India

Xiao Chenxia†, Xu Tianlv†, Steven Robert Kirk† and Samantha Jenkins*†
National and Local United Engineering Laboratory for New Petrochemical Materials and Fine Utilization of Resources, Key Laboratory of Chemical Biology and Traditional Chinese Medicine Research (Ministry of Education of China), Key Laboratory of Resource Fine-Processing and Advanced Materials of Hunan Province, College of Chemistry and Chemical Engineering, Hunan Normal University, Changsha, Hunan 410081, China

The topological diversity of sets of isomers of water clusters $(W = H_2O)_n$, $7 \leq n \leq 10$, is analyzed employing the scalar fields of total electronic charge density $\rho(\mathbf{r})$ and the molecular electrostatic potential (MESP). The features uncovered by the MESP are shown to be complementary to those revealed by the theory of atoms in molecules (QTAIM) analysis. The MESP is known to exhibit the electron localizations such as lone pairs that are central to water cluster behavior. Therefore, a 'hybrid' QTAIM and MESP quantum topology phase diagram (QTPD) for W_n, $7 \leq n \leq 10$, is introduced in addition to the QTPD. The 'spanning' QTPD with upper and lower bounds is constructed from the solutions of the Poincaré–Hopf relation involving the non-degenerate critical points. The changing subtle balance between the planar and three dimensional character of the growing water clusters W_n, $4 \leq n \leq 10$, is revealed. Characterization of the structure of the QTPDs, possible with new tools, demonstrated the migration of the position of the global minimum on the spanning QTPD from the lower bound to upper bound as the W_n, $4 \leq n \leq 10$, cluster grows in size. Differences in the structure of the QTPD are found between the clusters containing even versus odd monomers for W_n, n = 7-10. The energetic stability of the clusters which possess even number of monomers *viz.* n = 8,10 is higher than that of the n = 7,9 clusters due to relatively higher numbers of hydrogen-bond *BCP*s in the n = 8,10 clusters, in agreement with energetic results reported in the literature. A 'hybrid' QTPD is created from a new chemical relation $b_{HB} + l \geq 2n$ for W_n that relates the number of hydrogen-bond bond critical points (b_{HB}) with the number of oxygen lone pairs exclusively specified by the negative valued MESP (3,+3) critical points (l). The topologies of the subset $b_{HB} + l = 2n$ for W_n, point the way to the discovery of unknown 'missing' lower energy isomers. A discussion of the relative merits and range of applicability of the QTAIM and hybrid-QTPD analyses is included and concludes that the hybrid-QTPD analysis for W_n, is more useful for the association with the energy minima on the potential energy surface.

I.INTRODUCTION

Water clusters are systems of great importance to theoretical and experimental chemists due to their complex and peculiar chemical behavior. Extended hydrogen-bond networks in water clusters hold the key to all their subtle properties.[1] Understanding the nuances of hydrogen-bonding in water clusters is a preliminary step towards dissecting the properties of bulk water.[1] Several empirical models of potential energy surface have been proposed for water, for which empirical potentials have been fitted to experimental data.[1–4] Unfortunately, most of them fail to reproduce all the properties of water. Nevertheless, these empirical potential models are found to be adequate for estimating some bulk properties of water such as molecular solvation, heat of vaporization etc. Accurate energy and structure predictions are a formidable task using such model potential.[5] Huge advancements in computational resources in the recent years have enabled the use of *ab-initio* calculations of reasonably large water clusters such as W_n, n = 16, at a high level of correlated theory. Such theoretical studies get assertion from gas phase high resolution spectroscopic experiments. The potential energy surface (PES) of water possesses however, numerous local minima with soft modes due to the weak and extended hydrogen-bonding network.[1] The number of such local minima increases significantly with the increase in the size of the cluster making the search for global minimum difficult to rationalize. Graph theoretical procedures have recently been employed to predict possible number of local minima of water clusters possessing different hydrogen-bonding networks.[6–8] The upper bound on the number of graphs possible for a small cluster such as W_n, n = 8 was shown to be[6] 1929. Other methods for generating local minima of water include Monte Carlo sampling and Monte Carlo-based simulated annealing procedures.[6–8] Although graph theory can quantify the mathematical complexity of the potential energy surface it does not provide any insights into the changing balance between the different structural preferences as a cluster grows. For instance, there is a known transition between an energetic preference for planar structures for W_n, n = 4,5 to three dimensional morphologies for n = 6. An energy focused approach can determine both the complexity of the potential energy surface and the lowest energy structure. The energy based approach after having supplied the lowest energy structure for a given cluster size however, cannot provide insights into why a particular morphology is preferred. Insights can be gained by supplementing the energy focused approach with an investigation based for instance, on the topological analysis of electron density. Previously, just such a topological-energy paired investigation was found capable of explaining the W_n, n = 4-6 transition. The quantum theory of atoms in molecules is used to replace Euclidean based intuition, the dimensionality of a molecule, i.e. planar (2-D) or compact (3-D) is determined by the use of quantum mechanically consistent principles.

The focus of this work is to pair the traditional energy based approach with a topological one, in the first instance, the total electronic charge density $\rho(\mathbf{r})$ and then a hybrid approach involving molecular electrostatic potential (MESP) as well. Because the isomer sets comprise isolated minima, it is not possible to directly map the individual topologies to the potential energy surface. It has been already seen however, from the QTPDs constructed from the quantum theory of atoms in molecules (QTAIM) that one can get an overall view of a set of isomers with respect to the potential energy surface by the construction of 'spanning' quantum topology phase diagrams (QTPDs) with upper and lower bounds.[9–11] A so called spanning QTPD is constructed to 'span' the most likely range of possible topologies. Earlier, such an

investigation for W_n, n = 4-6 was undertaken, wherein the position of the global minimum was found to be dependent on the isomer size. In this way, it was possible to map the entire known topology solution space as a unit to the potential energy surface. In the present work, we revisit W_n, n = 4-6 in more detail and construct QTPDs for W_n, n = 7-10 and investigate their structure and relative position of the global minimum for each QTPD. We will also examine the variation of balance between the planar and compact characteristics with cluster size and to anticipate changes in the topology for smaller cluster sizes. Another application of these scalar fields is to be able to anticipate changes in the topology before it is evident in from the calculation of the energies alone. The use of QTPDs enables a new simultaneous overview of all known and unknown but possible isomer sets regardless of energetic stability that is not possible using purely energy based methods.

The QTAIM analysis quantifies the hydrogen-bonding, whereas the electron localization such as lone pairs on oxygen is revealed by the scalar field of MESP. In view of this, the present study introduces the concept of hybrid-QTPD which exploits the complimentary topological features from the QTAIM analysis and MESP. Such an approach paved a way to map the various energy minima of PES and gain insights into role of balance between lone pairs and hydrogen-bonds in determining the energetic stability of the isomers.

Further, the extra energetic stability of even numbered water clusters,[4] as reported in literature, has also been verified by scrutinizing the trend of the above mentioned analysis in terms of hydrogen-bond and lone pairs in the W_n, n = 7-10 water clusters.

II.THEORETICAL BACKGROUND

Investigation of hydrogen-bonding, lone pairs and energetic stability of water cluster is performed using critical points of two scalar fields namely total electronic charge density $\rho(\mathbf{r})$ and molecular electrostatic potential (MESP). A brief introduction to the topological features of from QTAIM and MESP is given below.

(i) *The Quantum Theory of Atoms in Molecules (QTAIM)*

Bader and coworkers pioneered the development of the quantum theory of atoms in molecules (QTAIM),[12] based on the scalar field of the total electronic charge density distribution $\rho(\mathbf{r})$ for molecules, clusters and solids.[9,13,14] Using QTAIM, several chemical phenomena such as the chemical bond, ellipticity of the bond ε, existence of atom in a molecule,[12] metallicity $\xi(\mathbf{r}_b)$ [15–17] and stiffness S.[18] For an N-electron system, described by the wave function, $\Psi(\mathbf{x}_1,\mathbf{x}_2,\ldots\mathbf{x}_N)$, with $\mathbf{x}_i$ denoting the combined space-spin coordinates of electron i, the total electronic charge density $\rho(\mathbf{r})$ can be written as

$$\rho(\mathbf{r}) = N \sum_{\sigma} \int \left|\psi(\mathbf{x}, \mathbf{x}_2, \ldots \mathbf{x}_N)\right|^2 d^3 r_2 \ldots d^3 r_N \qquad (1)$$

The salient features of this scalar field in Equation (1) are discovered by mapping out the critical points and the gradient paths connecting the critical points.[12] Four distinct types of non-degenerate critical points appear in the QTAIM topology. The critical point is defined as a location in field where all the partial first derivatives of the function vanishes *i.e.* $\nabla\rho(\mathbf{r}) = 0$. Further, the nature of these critical points is revealed out by the three eigenvalues (λ_1, λ_2 and λ_3) of the

corresponding Hessian matrix. These critical points are labeled using the notation (R, •) where R is the rank of the Hessian matrix, the number of distinct non-zero eigenvalues and • is the signature (the algebraic sum of the signs of the eigenvalues). A (3, -3) critical point denotes a maximum and usually corresponds to a nuclear position. Non-nuclear maxima however, have also been reported in the QTAIM topology of alkali metal clusters.[19] A minimum *i.e.* (3, +3) critical point corresponds to a cage, generally referred to as cage critical point (*CCP*). The saddle points *viz.* (3, -1) critical point and (3,+1) critical point are exclusively associated with topological bond and ring respectively. Thus, a (3,-1) critical point is also referred to as bond critical point (*BCP*), whereas (3,+1) critical point is called ring critical point (*RCP*). There exist several gradient paths, which originate and terminate at the critical points. Specifically, a pair of gradient paths connecting a *BCP* to two adjacent nuclei, for which ρ is a maximum with respect to any neighboring path, is known as an atomic interaction line (AIL). The two connected nuclei are said to be linked by a bond-path, which corresponds to a chemical bond. Early work by Bader and co-workers [20] drew on the mathematical work of Collard and Hall, [21] Johnson [22] and Smith [23] to capture the essential nature of a molecule into a suitably simple form in real space: the *molecular graph*, which is defined as the set of critical points and the associated bond-paths. The molecular graph provides a topological overview of the characterizing chemical features derived from a many-body space, replacing the concept of geometrical degrees of freedom. The ellipticity, ε provides relative accumulation of charge in the two directions perpendicular to the bond-path at a *BCP*, defined as $\varepsilon = (|\lambda_1|/|\lambda_2| - 1)$ where λ_1 and λ_2 are the negative eigenvalues of the corresponding Hessian matrix at the *BCP*.[12] Further, the evaluation of the Laplacian $\nabla^2\rho(\mathbf{r})$ at the *BCP* shows the distinction between the non-covalent, ionic and covalent bonds.[12] To address the issue of cooperativity in hydrogen-bonding we use $H(\mathbf{r}_b)$, the local total energy density at the *BCP* suggested by [24]:

$$H(\mathbf{r}_b) = V(\mathbf{r}_b) + G(\mathbf{r}_b) \qquad (2)$$

Where $V(\mathbf{r}_b)$ and $G(\mathbf{r}_b)$ are the local potential and kinetic energy densities at the *BCP* respectively. Previously, one of us found that the usual strength of hydrogen-bonds in ice I_h could be explained in terms of Equation (2),[13] in agreement with the experiment, [25] where a degree of covalent character is indicated by $H(\mathbf{r}_b) < 0$.

For consistency, we use quantum geometry-centered rather than Euclidean geometry-centered intuition to determine whether a molecular graph is 3-D_{QT}, 2-D_{QT} or 1-D_{QT}, where sub-script '$_{QT}$' is used to denote quantum topology. Molecular graphs of molecules or clusters with one or more *CCP*s will be considered to be quantum topologically 3-D_{QT}. Similarly, 2-D_{QT} and 1-D_{QT} refer to molecular graphs possessing at least one *RCP* (no *CCP*) and one *BCP* (no *RCP* and *CCP*) respectively.

(ii) *Molecular Electrostatic Potential*

The scalar field of molecular electrostatic potential (MESP) and the associated topography[26–35] provides an essential tool for studying existence of lone pairs,[28] hydrogen-bonding,[29,30] molecular reactivity[31,32] etc. The MESP topography is richer as compared to that from the QTAIM analysis in terms of the number of critical points. The MESP, V(**r**), see Equation

(3), generated by such a system having N nuclei with charges $\{Z_A\}$ located at $\{\mathbf{R}_A\}$, and the total electronic charge density $\rho(\mathbf{r})$ at a point $\mathbf{r}$ in space is given by:

$$V(\mathbf{r}) = \sum_{A}^{N} \frac{Z_A}{|\mathbf{r} - \mathbf{R}_A|} - \int \frac{\rho(\mathbf{r}')\, \mathrm{d}^3\mathrm{r}'}{|\mathbf{r} - \mathbf{r}'|} \tag{3}$$

Analogous to the QTAIM topography, the salient features of MESP are succinctly summarized the four non-degenerate critical points. Pathak and Gadre[33] have rigorously proved the absence of non-nuclear maxima in MESP. Thus, a (3,-3) critical point is exclusively associated with the nuclear positions. A (3,-1) critical point in MESP represents a bond and may additionally connect two (3,+1) critical points. The other type of saddle, *viz.* (3,+1) critical point is associated with topographical ring as is the case for QTAIM, but can also be formed between two topographical minima. MESP contains critical information about electron localization in a molecular system. Electron localization highlighted by negative-valued (3,+3) critical points in MESP unlike the QTAIM topography. The topographical cages are generally represented by positive-valued (3,+3) MESP critical point. The MESP value at the location of negative valued (3,+3) critical point is indicative of the strength of the localization and has been used to predict the energetic stability of various non-covalently bound molecular systems. A method has been recently proposed to identify the negative-valued (3,+3) critical points associated exclusively with the lone pairs (*LCP*s), based on eigenvalue and associated eigenvector of the corresponding Hessian matrix.[28] The Poincaré-Hopf relation for MESP is provided in terms of the number of non-degenerate critical points[34–36] by the following equation:

$$n_{+3} - n_{+1} + n_{-1} - n_{-3} = \chi = n_{-} - n_{+} \tag{4}$$

On the left hand side of Equation (4), n represents the number of and the subscript corresponds to signature of non-degenerate critical point, while n_{-} and n_{+} on right hand side denotes the number of asymptotic maxima and minima of the scalar field respectively. In contrast to the $\rho(\mathbf{r})$, χ for MESP varies from system to system and is evaluated by counting the numbers of closed *island-like* regions of negative (*asymptotic maxima*) and positive (*asymptotic minima*) MESP on a sufficiently large sphere centered at the center of mass of the molecule.[35]

(iii) *The Quantum Topology Phase Diagram (QTPD)*

In reference to the total electronic charge density $\rho(\mathbf{r})$ the Poincaré–Hopf relation can be written as:

$$c - r + b - n_{cp} = \chi \tag{5}$$

where the χ denotes the Euler characteristic. The variables c, r, b and n_{cp} correspond to the number of *CCP*s, *RCP*s, *BCP*s and *NCP*s respectively, where the sum of first three types of critical points defines the topological complexity of a molecular graph. The total charge density $\rho(\mathbf{r})$ is a positive semi-definite scalar field, for which the Euler Characteristic χ

= -1, for any molecule or cluster and correspondingly $\chi = 0$ for a solid. The sum Σ_{brc} provides us with a measure of the overall topological complexity of a molecular graph, the high the sum the higher the topological complexity.

Previously, some of the current authors have represented the QTAIM topologies of sets of isomers of allowed, forbidden and unstable solutions to Poincaré-Hopf relationship given by Equation (5), using the quantum topology phase diagram (QTPD).[9–12] For a given collection of isomeric molecular graphs, the number of *BCP*s and *RCP*s given by *b* and *r* respectively, contained in each molecular graph are plotted along the *x*-axis and *y*-axis. Due to the integer nature of the solution set of the Poincaré–Hopf relation there is a restriction on the range in the QTPD for the topologies of isomers of a given chemical system. It should be noted that the topologically stable as well as 'missing' topologies which fall in hypothesized stable zone of QTPD may have one or more local energy minima associated with them. These missing topologies may correspond to various types of stationary points in the PES: stable minima, transition states etc. Finally, topologically unstable solutions are increasingly unlikely to be found as molecular graphs due to the increasing number of *CCP*s. We attempt to construct a complete QTPD in terms of the ranges of values of *b* and *r,* that we refer to as a *spanning* QTPD. This is undertaken by determining the upper and lower boundaries of the QTPD for values of *b*, the lower boundary defined by where the number of *BCP*s and *NCP*s are equal. The upper boundary of the spanning QTPD is defined as the simplest regular polyhedron constructible. In this work we do not consider the string like solutions string-like solutions of the Poincaré-Hopf relationship where $r = 0$.

The charge density distribution $\rho(\mathbf{r})$ around critical points and their relative positions are indicators of the topological stability of the dimensionality of the molecular graph. For example, the topological stability of *BCP*s and *CCP*s have been verified to be related to the location, relative to the closest *RCP*.[10] The significance of this is that the coalescence and subsequent annihilation of the sole *RCP* of a 2-D_{QT} molecular graph with a close *BCP* will reduce to quantum topology from 2-D_{QT} to 1-$D_{QT.}$ Similarly the loss of the only *CCP* of a 3-D_{QT} by coalescence with an *RCP* will render the molecular graph 2-$D_{QT.}$

Recent work on QTPDs has included non-nuclear attractors (*NNA*s) by incorporating a third axis either of the number of *CCP*s or *NNA*s. [37] Also the treatment of sets of non-isomeric species as would be found in a reaction cycle. In the present work, we focus on the topologies of isolated minima and so it is not possible to relate the positions of each of the locations on the QTPD with the potential energy surface.

Because the QTPD approach is not specific to the total electronic charge density distribution $\rho(\boldsymbol{r})$ it could work equally well with other scalar fields for instance the Ehrenfest Force partitioning, [38] and MESP. The asymptotic topological behavior of any function is provided by the Euler characteristic. The latter puts restriction on the various combinations of non-degenerate critical points of these scalar fields, as provided by the Poincaré-Hopf relation, see Equation (5). It turns out that the solution space of a QTPD, unlike the terrain of potential energy surface, is more confined and has the possibility for predicting new topologies of the QTAIM, Ehrenfest or MESP fields. We are particularly interested in including an analysis of the oxygen lone pairs as revealed by MESP, central to both hydrogen-bond formation in water clusters and the cluster morphologies. Unfortunately, a pure MESP QTPD is not practical because of divergent chemical

significance of any particular type of non-degenerate critical point as well as varying Euler characteristic values; 0, ±1, ±2 etc., would necessitate an additional axis to be added to a QTPD to represent each additional Euler characteristic value. It is both however, possible and practical to create a 'hybrid' QTAIM-MESP QTPD that can include the oxygen lone pair topologies. A hybrid-QTPD is created by plotting the number of lone pairs (l) obtained from MESP topology against the number of hydrogen-bond *BCP*s (b_{HB}) obtained from a QTAIM analysis. All the isomers of a particular water cluster are spanned over such a hybrid-QTPD providing yet another comprehensive method of mapping the numerous energetic minima in PES. Similar to the QTPD, each point on a hybrid-QTPD can refer to one or more energetic minima. These points however, can be fuzzily associated with distinct relative energy zones of isomers of W_n. The position of global minimum in hybrid-QTPDs of W_n, n = 7-10 is found to be strongly associated with a particular region, the lower right, unlike the QTPD where it is variable. Further, the hybrid-QTPD shows that the isomers are restricted to a hypothesized zone of energetic stability based on a relation between the number of lone pairs (l) and hydrogen-bond *BCP*s (b_{HB}). The consequence of this is that certain combinations l and b_{HB} are more likely to be found in stable water clusters. In this work we refer to a QTPD derived purely from QTAIM properties as a *QTPD* and a QTPD derived using a combined QTAIM and the MESP analyses as a *hybrid-QTPD*. If a hybrid topology possesses an Euler Characteristic χ = -1 then the hybrid topology can be mapped directly *back* on the QTPD to extract the QTAIM topologies b, r and c. Therefore, the consideration of the Euler Characteristic χ = -1 may be useful for identifying features of 'missing' hybrid-QTPD topologies of more energetically stable structures. Such features could include the quantum dimensionality, i.e. if the topology corresponds to a 2-D_{QT} or 3-D_{QT} molecular graph. Discrepancies will arise where molecular graphs contain O---O *BCP*s since it will no longer be possible to assume $b = b_{HB} + 2n$. Therefore, as part of the QTAIM investigation we will search for the presence of O---O *BCP*s and examine the relative energetic stability of the corresponding isomers compared with isomers that do not contain O---O *BCP*s.

III. COMPUTATIONAL METHODS

Isomers of the water clusters W_n, n = 7-10 are considered for the present topological study. The initial geometries are obtained from cluster builder[39] which uses electrostatic guidelines to build upon clusters of smaller sizes. Molecular cluster builder involves addition of a monomeric unit onto the favorable locations in the parent cluster. The monomeric unit to be added is treated as a set of point charges in the sea of the electrostatic potential created by the parent cluster. The negative-valued minima in MESP distribution are used to position the positive-point charges of the monomer, such that the energy of the new cluster is minimized. Previously reported structures of energy minima[40] have also been incorporated in the study in order to ensure no relevant energy minima are missed. These starting geometries of water clusters are initially optimized at B3LYP/6-31+G(d). The structures of local minima obtained on optimization are further subjected to geometry optimization at MP2/aug-cc-pvDZ level of theory. Theoretical investigation of hydrogen-bonding demands appropriate treatment of electrostatic, dispersion, induction and exchange energies. Coupled cluster methods are indeed known to perform well for evaluating these components, but unfortunately become prohibitively expensive for large molecular clusters. On the other hand, MP2 method (despite overestimating the dispersion interaction) still proves to

be quite reasonable level of theory for studying water clusters. All the *ab-initio* calculations on clusters are performed using Gaussian09 package. The density matrix obtained at MP2/aug-cc-pvDZ has been employed to perform the QTAIM and MESP analysis. The QTAIM analysis is performed using AIMQB within the AIMAll package[41]. The location and characterization of the MESP critical points is carried out using the topography mapping Fortran code developed recently by Yeole *et al*.[42] The program takes as input, a set of guess points, provided by critical points of the bare nuclear potential (BNP) and the total electronic charge density $\rho(\mathbf{r})$. Initial guess points are optimized using L-BFGS code, based on quasi-Newton methods. The deformed atoms in molecules (DAM) procedure proposed by Rico and López *et al*.[43] is implemented for evaluating values of $\rho(\mathbf{r})$ and the MESP and their corresponding first and second partial derivatives at a given point. The DAM method, based on partitioning of total electronic charge density $\rho(\mathbf{r})$ into atomic contributions, provides a rapid and sufficiently accurate function and gradient calculation.

IV. RESULTS AND DISCUSSION

(i) *QTAIM Analysis*

The molecular graphs of the global minimum (GM) of each of the W_n, n = 7-10, QTPDs are shown in Figure 1(a-d) along with the molecular graphs of equal or higher topological complexity Σ_{brc}, defined as the sum of the numbers of *BCP*s, *RCP*s and *CCP*s, given by the variables b, r and c respectively. In addition, a selection of the QTAIM and MESP properties of the W_n, n = 7-10, molecular graphs including the numbers of hydrogen-bond *BCP*s (b_{HB}) and *LCP* critical points corresponding to the oxygen lone pairs (l) are presented with the relative energies $\mathbf{\Delta E}$ in Tables 1-4. The complete QTAIM and MESP data set is provided in Tables S1-S4 of the Supplementary Materials.

For W_n, n = 7-10 the number of relatively low lying isomeric minima which possess *CCP*s (c) increases with the increase in water cluster size. For W_n, n =7 the molecular graph corresponding to the energetically low lying structures have a *CCP*, for n = 8 and n = 9 the first five and six most energetically stable molecular graphs respectively possess *CCP*s. For W_n, n = 10 most of the molecular graphs tend to possess a *CCP* demonstrating the increasing dominance of the 3-D_{QT} character with increase in cluster size. Note also W_n, n = 6, provided from a previous investigation also possess 3-D_{QT} character. Thus, an inspection of Table 5 highlights the affinity of the water cluster molecular graphs towards 3-D_{QT} character with increase in cluster size from W_n, n = 6-10, see Tables 1-4.

Examination of the correlation between the energetic stability for W_n, n = 7-10 and topological complexity Σ_{brc} shows reasonable but not universal agreement, see Tables 1-4. Therefore, the topological complexity Σ_{brc} is not a particularly reliable method to index the QTPD on the basis of the potential energy surface. For the W_n, n = 8,10 clusters the molecular graphs of the global minimum possess geometries close to that of a regular polyhedron. This is not the case for W_n, n = 7-9, where none of the molecular graphs, including the global minimum, possess regular polyhedral geometries. For W_n, n = 6,8,10 the presence of global minimum with possessing geometries with a regular polyhedron form has implications in both in terms of the number density ($b_{HB}/2n$) and stability of the hydrogen-bond *BCP*s that are formed. Within QTAIM the stability is determined by the total local energy density $H(\mathbf{r_b})$ that we will discuss later in this section. Equivalently, in section (ii) *MESP analysis* we explain why additional numbers of weak or malformed hydrogen-bond *BCP*s do not result in structures with greater energetic stability.

A closer examination Poincaré-Hopf solutions, that now includes a breakdown between 2-D_{QT} and 3-D_{QT} is presented in Table 5. For QTPD of W_n, n = 4 the total number of distinct solutions for the Poincaré-Hopf relation is only three compared to five and six for n = 5,6 clusters respectively. For the current set of newly investigated QTPDs; W_n, n = 7-10, n = 7 has the same total number of Poincaré-Hopf solutions as n = 6, but there is a *decrease* for n = 8 to only five solutions and n = 9 shows a further decrease to only four. This trend is only reversed with increase in cluster size for W_n, n = 10 where the total number of solutions of the Poincaré-Hopf relation increases to nine. It can be seen for W_n, n = 7,9 that there is a levelling off and then a *decrease* in the number of 3-D_{QT} Poincaré-Hopf solutions. Of the W_n, n = 4-10 QTPDs, it is the n = 10 QTPD that uniquely possesses greater numbers of 3-D_{QT} Poincaré-Hopf solutions than 2-D_{QT} Poincaré-Hopf solutions indicating a transition to compact topology behavior.

For the QTPDs, missing topologies are shown as red squares on Figure 2 could correspond to transition states, IRCs, excited states, charged clusters or those not obeying the Bernal Fowler ice rules. If a missing hybrid-QTPD topology possess an Euler Character χ = -1, then it can be mapped back to a missing QTAIM topology via the b_{HB} value from the hybrid-QTPD, remembering to add on 2n to account for the O-H sigma *BCP*s, see section (ii) *MESP Analysis*. In terms of selecting for more energetically stable isomers this is unlikely to be problematic as the most energetically stable isomers studied so far; W_n, n = 4-10 and n = 12 do *not* contain O---O *BCP*s, see Tables 1-4 and Table S6 of the Supplementary materials. We consider the global minimum of W_n, n = 8, the H20-8-1 isomer as an example of where the hybrid-QTPD has an Euler Characteristic χ = -1, see Table 2 and Figure 5(b). The hydrid-QTPD topology (b_{HB} = 12, l = 4) corresponds to a QTAIM topology (b = 28, r = 6, c = 1), from this we see that the molecular graph possesses a 3-D_{QT} quantum topology i.e has a compact form, see Figure 2(b).

To explain this seemingly contradictory behavior of the decrease in the number of Poincaré-Hopf solutions with increase in isomer size for W_n, n = 7,9 we introduce the QTPD structure measures D_L and D_U for n = 4-10. The measures D_L is defined to be the separation along the b-axis from the lowest boundary b = 3n, where n corresponds to the number of water monomers and not the number of nuclei, *NCP*s (n_{cp}), of the QTPD and the global minimum, see equation (5). For D_L the number of *RCP*s, r = 1, corresponding to the least topologically complex, non-string-like, molecular graph possible. For the QTPDs of W_n, n = 4,5 we see D_L = 0, where the global minimum are at located at (12,1) and (15,1) on

the respective QTPDs, i.e. the topology of the global minimum in each case coincides with $b = 3n$. This is in contrast to W_n, n = 6-10 where $3 \leq D_L \leq 5$. The value for $D_L > 0$ for all the QTPDs of W_n, n = 6-10 indicate a general trend towards increasingly compact molecular graphs with increase in cluster size n. For example for W_n, n = 7 it can be seen that $D_L = 3$ from Figure 2(a), see also Table 5. It can be noticed that each of the QTPDs of W_n, n = 4-10 possesses at least one 2-D_{QT} molecular graph, see Figure 2.

The possible numbers of hydrogen-bond *BCP*s is denoted by the integer b_{HB} for each of the QTPDs of W_n, n = 4-10 and is given in Table 5, where n is number of water monomers in each cluster W_n. Notice, that as the size of the water clusters increases the lowest relative permitted value of b_{HB} increases. For example for W_n, n = 10, the less complex combinations; n, $n + 1$ or $n + 2$ of hydrogen-bonding are no longer permissible despite the existence of 2-D_{QT} molecular graphs for n = 10, indicating the start of the transition to all compact (3-D_{QT}) topologies.

An examination of the Poincaré-Hopf solutions by cluster size shows that only the molecular graphs of W_n, n = 9 do not possess any O---O *BCP*s, see Table 1-4. This may be related to the lack of topological complexity of W_n, n = 9, having only four distinct QTAIM topologies on the QTPD, see Figure 2. This finding is in agreement with earlier work on the W_n, n = 4-6 QTPD; for n = 4 there were only three distinct topologies none of which contained O---O *BCP*s. This was despite the existence of a very strained and high energy 3-D_{QT}, n = 4 molecular graph. Therefore, we can suggest that the O---O *BCP*s arise as a consequence of topological variability. The property of topological variability is not evident until we map out *all* of the known isomers of a given size, not just the global minimum. We can see that the most topologically variable QTPD is that of W_n, n = 6, from Table 5 where we can see seven possible values of b_{HB}. The consideration of the isomers other than the global minimum, shown in a non-bold font in Table 5, enables the progression from W_n, n = 4-10 to be seen in terms of both lower and higher values b_{HB}.

The complementary QTPD structure measure D_U is defined to be the separation of global minimum and the defined upper limit of the QTPD and describes the relative change in positions of the global minimum, see Table 5. For W_n, n = 4,5 it can be remembered that the global minimum was located at $D_L = 0$ and the n = 6 global minimum was located at the geometric center of the QTPD, corresponding to $D_U = 3$. For the present work $D_U > 0$ for the QTPDs with odd numbers of monomers, W_n, n = 7,9, as was the case for n = 4-6. This is in contrast with the W_n, n = 8,10 QTPDs where in each case $D_U = 0$. For W_n, n = 8,10 the topologies of the global minima correspond to regular polyhedron for n = 8 and n = 10 the geometries correspond to a cube and pentagonal prism respectively, see Figure 1 and Table 5. We notice that the QTPD of W_n, n = 10 displays the unique characteristic of possessing Poincaré-Hopf solutions *beyond* the defined upper defined QTPD boundary, none of the n = 4-9 QTPDs display this behavior, see Figure 2(d).

In the earlier investigation by some of the current authors[10], an increase in cooperativity effects in the W_n, n = 4-6 isomers with cluster size were found using $H(\mathbf{r}_b) < 0$ for hydrogen-bond *BCP*s to indicate a degree of covalent character. An examination of the values of $H(\mathbf{r}_b)$ and the relative numbers of hydrogen-bond *BCP*s can reveal additional insights into the different behavior of the water clusters with even or odd values of n. We can also investigate the ratio $b_{HB}/2n$ of the number of hydrogen-bond *BCP*s (b_{HB}) for W_n, n = 4-10, which is effectively the hydrogen-bond *BCP* density, see Table 5.

It is impossible for a chemically meaningful structure to utilize all the lone pairs (*LCP*) and hydrogen atoms forming 2*n* hydrogen-bond *BCP*s, see section (ii) *MESP Analysis*. We can however investigate (indirectly) the effects of this property by constructing the ratio $b_{HB}/2n$ of the number of hydrogen-bond *BCP*s for W_n, n = 4-10, effectively the hydrogen-bond *BCP* density, see Table 5. In the unattainable limit of all lone pairs being utilized the hydrogen-bond *BCP* density, $b_{HB}/2n = 1$. The oxygen lone pairs however, are central to this behavior and are beyond the scope of QTAIM analysis and therefore we will investigate further why the hydrogen-bond *BCP* density, $b_{HB}/2n < 1$ for W_n, n = 4-10, see section (ii) *MESP Analysis*. Here, for W_n, n = 7-10 we again use $H(\mathbf{r}_b) < 0$ to indicate a degree of covalent character and we find that the clusters n = 8,10, have a higher degree of covalent character, seen by more values of $H(\mathbf{r}_b) < 0$, see Figure 3. Referring again to the earlier work on the W_n, n = 4-6 isomers it can be noticed that the n = 6 isomer set has more values of $H(\mathbf{r}_b) < 0$ than does n = 7,9. In addition, the isomer sets of W_n, n = 6,8,10 have the highest values (0.75) of the hydrogen-bond *BCP* density ($b_{HB}/2n$) compared with n = 7,9 (0.71 and 0.72 respectively). This finding is in agreement with earlier work that found that for W_n, n = 7-16, the energetic stability was found to increase due to a large value of b_{HB} for clusters with an even number of monomers[44], although we notice that W_n, n = 6 should also be included on the basis of the values of $H(\mathbf{r}_b) < 0$ and on the hydrogen-bond *BCP* density ($b_{HB}/2n$) values.

Table 5. The analysis of Poincaré-Hopf solution set for W_n, n = 4-10. The entries D_L and D_U refer to the *separation* of the global minimum (GM) from the lower and upper boundaries of the spanning QTPD respectively. See section **II (iii)** for the definitions of the upper and lower boundaries of the QTPD. Under the headings '2-D_{QT}' and '3-D_{QT}' are the number of unique Poincaré-Hopf solutions, the sum '2-D_{QT}' + '3-D_{QT}' is presented under the heading 'Total'. The variable b_{HB} represents the number of hydrogen-bond *BCPs* for the W_n, n = 7-10 QTPDs; values of b_{HB} corresponding to the global minimum are indicated in a bold font. The presence of O---O *BCP*s is indicated by the entry being underlined. The ratio $b_{HB}/2n$ gives the hydrogen-bond *BCP* density for the global minimum of each QTPD.

			Unique Poincaré-Hopf Solutions					
QTPD	D_L	D_U	*Polyhedron*[a,b]	2-D_{QT}	3-D_{QT}	Total	b_{HB}[c] for W_n, n = 4-10	$b_{HB}/2n$
$W_{n=4}$	0	2	Tetrahedron	2	1	3	$\boldsymbol{n+0}$, $n+1$, $n+2$	**0.50**
$W_{n=5}$	0	4	Triangular bipyramid	3	2	5	$\boldsymbol{n+0}$, $n+1$, $\underline{n+3}$, $\underline{n+4}$	**0.50**
$W_{n=6}$	3	3	Octahedron	3	3	6	$n+0$, $\underline{n+1}$, $\underline{n+2}$, $\boldsymbol{n+3}$, $\underline{n+4}$, $\underline{n+6}$	**0.75**
$W_{n=7}$	3	2	Augmented triangular prism	3	3	6	$n+1$, $\underline{n+2}$, $\underline{\boldsymbol{n+3}}$, $n+4$	**0.71**
$W_{n=8}$	4	0	Cube(GM)	3	2	5	$n+2$, $n+3$, $\underline{\boldsymbol{n+4}}$	**0.75**
$W_{n=9}$	4	1	Tridiminished icosahedron[b]	3	1	4	$n+2$, $n+3$, $\boldsymbol{n+4}$	**0.72**
$W_{n=10}$	5	0	Pentagonal Prism(GM)	4	5	9	$n+3$, $n+4$, $\boldsymbol{n+5}$, $\underline{n+6}$, $\underline{n+7}$	**0.75**

[a] For $W_{n=7}$ the estimated upper boundary of the QTPD (26,7) is located to the right of the global minimum (GM).
[b] For $W_{n=9}$ the estimated upper boundary of the QTPD (32,7) is located to the right of the global minimum (GM).
[c] The results for the analysis of the number hydrogen-bond *BCP*s (b_{HB}) for W_n, n = 4-6 have previously been published but are listed here for the sake of comparison.

(ii) *MESP Analysis*

The capabilities of the MESP complement the QTAIM analysis for verifying the reasons for energetic stability of the water clusters W_n, n = 7-10. The relative energetic stability of a water cluster is loosely determined by the number of hydrogen-bonds. The number of hydrogen-bonds is determined using QTAIM in terms of the numbers of hydrogen-bond

*BCP*s (b_{HB}), see Tables 1-4. It is clearly revealed that some of the water clusters in spite of possessing fewer hydrogen-bond *BCP*s (b_{HB}) may be more energetically stable, see Tables 1-4, note that *b* in the Tables is the *total* number of *BCP*s including sigma O-H and O---O *BCP*s. The discrepancy as to why some of the water structures are more energetically stable despite possessing fewer hydrogen-bond *BCP*s is resolved through further MESP analysis. Before embarking on the MESP analysis of water clusters, it is important to describe the topological characteristics of a single water molecule and the associated dimer; the simplest cluster. A single molecule of water possesses two negative (3,+3) MESP critical points corresponding to the lone pairs on the oxygen atom of H_2O. The two oxygen *LCP*s are connected through an intervening (3, +1) MESP saddle point. The typical MESP value at these *LCP*s at MP2/aug-cc-pvDZ level of theory is approximately -45 kcal/mol, reflecting the strength of the lone pair. Hydrogen-bond formation in a water dimer involves a weak interaction between one of the two *LCP*s of an H_2O molecule and the hydrogen atom of the other. This leads to the formation of a hydrogen-bond and the annihilation of the *LCP* involved in the interaction. There is a significant change in the MESP value of the 3 *LCPs* in the water dimer; the MESP minima in the H-donor H_2O moiety shows deepening of the MESP to -56 kcal/mol, while the H-acceptor molecule possesses MESP minimum of -31 kcal/mol. This indeed shows a significant amount of charge transfer from acceptor to donor molecule, involved in the hydrogen-bonding. This variation in MESP value highlights the cooperativity phenomenon, well-known in hydrogen-bonding of clusters.[29,30] In the QTAIM analysis we expressed cooperativity using the local energy density $H(\mathbf{r_b}) < 0$ for hydrogen-bond *BCP*s to indicate a degree of covalent character, see Equation (2) and Figure 3.

Similar characteristics have been observed in the bonding network in larger water cluster. The latter however, shows a distribution of negative MESP values among the (3,+3) MESP critical point*s*. A common feature of clusters possessing very small-valued (3,+3) critical points (MESP value > -18 kcal/mol) is observed in all the clusters irrespective of size and energetic stability order. They are remnants of *LCP*s and show some imperfection in the hydrogen bond formed. Even the most stable clusters in this study shows such small valued critical points reflecting the complex MESP created by various hydrogen and oxygen atoms in the cluster. On the other hand, there are some (3,+3) critical points within the range of -18 kcal/mol to -30 kcal/mol. Such critical points appear because certain hydrogen-bonds are formed through the interaction of hydrogen with a (3,+1) critical point of H_2O lying between two lone pairs instead of interaction with the lone pairs. When these weaker hydrogen-bonds form, the *LCP* remains intact, although the MESP value at corresponding *LCP* is less negative. We use the less negative value of the MESP associated with an *LCP* in the water dimer (-31 kcal/mol) to sort the distinct hanging lone pairs in the water cluster, which are projected on y axis of the hybrid-QTPD, as discussed below.

The MESP analysis of the W_n, n = 7-10 structures that includes the number of negative valued (3,+3) MESP critical points that correspond exclusively to the numbers of oxygen lone pairs *LCP*s (l) and b_{HB} are presented in Figure 4 and Tables 1-4. The corresponding molecular graphs from the QTAIM analysis are presented in Figure 1. It is clear that the maximum value for b_{HB} possible in a stable water cluster W_n is $2n$, where n is the number of oxygen atoms in the cluster. It is impossible however, for a chemically meaningful structure to utilize all the lone pairs and hydrogen atoms forming $2n$ hydrogen-bond *BCP*s. This implies that b_{HB} and the number of lone pairs (l) in water clusters are correlated, see Equation

(6). In view of this we introduce a hybrid-QTPD, wherein the variables of b_{HB} and l in all the isomeric forms of a water cluster are plotted against each other, see Figure 5 and Tables 1-4. Higher values of l correspond to more unutilized oxygen *LCP*s. For the hybrid-QTPDs all initial (lowest) values of $b_{HB} = n$, i.e. corresponding to the value required to form a linear chain isomer of water cluster consisting of n water monomers. In the construction of the hybrid-QTPD the lowest energy isomers are expected to follow the relation:

$$b_{HB} + l = 2n \qquad \text{for } W_n, \qquad (6)$$

where more stable clusters will tend to maximize the hydrogen-bond *BCP* density ($b_{HB}/2n$), resulting in a reduction of the value of l, the hybrid-QTPDs of the W_n, n = 7-10 clusters are shown in Figure 5. These hybrid-QTPDs can be observed to exhibit different characteristics as compared to the QTPDs. Instead of occupying the bottom right hand portion of the hybrid-QTPD, the 'forbidden' region now occupies the front left portion of the hybrid-QTPD, formed by those b_{HB}:l combination for which their sum is less than $2n$. As can be deduced from Equation (6), the plot is expected to have a negative slope, indicated by solid black line in Figure 5 with only one possible of value of l, for a given b_{HB}. However, this is not always the case and the hybrid-QTPDs demonstrate that isomers of a cluster W_n form a distribution of b_{HB}: l combination *i.e.* for a given value of b_{HB} there exists more than one possible value of l in various isomeric forms, see Figure 5. This implies that all of the isomers follow the relation:

$$b_{HB} + l \geq 2n \qquad \text{for } W_n \qquad (7)$$

where a sub-set of the isomers belong to:

$$b_{HB} + l > 2n \qquad \text{for } W_n \qquad (7a)$$

Nevertheless, amongst the isomers containing same value of b_{HB}, the most energetically stable follow Equation (6). Notice that for each of the hybrid-QTPDs of W_n, n = 7-10, all of the topologies of the respective global minimum satisfy Equation (6). All the structures with topologies that violate Equation (6) are relatively less stable and contain more of weak hydrogen-bond *BCP*s.

There are a few isomers in the W_n, n = 7-10 hybrid-QTPDs with topologies that violate Equation (6), i.e. they contain higher numbers of hydrogen-bond *BCP*s (b_{HB}) than those found in that of the topology corresponding to the GM but the energetic rank ordering places them nearly at the bottom of the list, see Tables 1-4 and Figure 5. The question of why the W_n, n = 7-10 structures that possess the maximum numbers of hydrogen-bond *BCP*s are not the most energetically stable or how is it possible in general to violate Equation (6) can be efficiently addressed using MESP topography. For example, the formation of a stronger $H(\mathbf{r}_b) < 0$, hydrogen-bond *BCP* is only possible where an *LCP* is utilized on an oxygen atom. Hydrogen-bonds that do not form through the interaction with an negative MESP (3,+3) *LCP*, lead to the formation of a weaker hydrogen-bond *BCP*s with $H(\mathbf{r}_b) > 0$. Such hydrogen-bond *BCP* formation does not utilize the *LCP* on an oxygen atom but instead through a (3,+1) critical point of H_2O lying between two lone pairs.

We now will give two examples of water structures that violate Equation (6), both involve the formation of weaker hydrogen-bond *BCP*s. For the first example we consider the W_n, n = 7 (H2O-7-t16) isomer satisfies Equation (7a) but not the more restrictive Equation (6), since b_{HB} = 11 and l = *5*. This occurs because the process of forming a weak, i.e. $H(\mathbf{r}_b) > 0$, hydrogen-bond *BCP* leads to 2 *LCP*s of the O13 of the W_n, n = 7 (H2O-7-t16) isomer being unutilized, see Figure 1(a) and Figure 4(a). For the second example we again see that the W_n, n = 10 (H2O-10-t13) isomer only satisfies Equation (7a) with b_{HB} = 15 and l = 7. This is because the O22 atom forms 3 hydrogen-bond *BCP*s due to the presence of the 2 *LCP*s and a (3, +1) critical point, see Figure 1(d). The O13 of W_n, n = 7 (H2O-7-t16) and O22 of n = 10 (H2O-10-t13) atoms that bind 'anomalously' whereby the two unutilized *LCP*s of the O13 and O22 atoms are indicated by the black arrows, see Figure 4(a) and Figure 4(d) respectively. Therefore, the W_n, n = 7-10 molecular graphs of this study that contain weak, $H(\mathbf{r}_b) > 0$, hydrogen-bond *BCP*s, whose formation results in unutilized oxygen lone pairs *LCP*s tend to be less energetically stable. By way of contrast, none of the structures of the global minimum (GM) of the W_n, n = 7-10 clusters contain hydrogen-bond *BCP*s whose formation resulted in unutilized oxygen *LCP*s. Another way to express this result is demonstrated in Table S5 of the Supplementary Materials where the value of (b_{HB}/l) is a maximum for each of the structures that correspond to global energy minimum.

Analogous to the QTPDs, the hybrid-QTPDs also indicate the presence of 'missing' topologies, related to the combinations of b_{HB} and l that could satisfy Equation (6). We have been able to divide the entire hybrid-QTPD into topologies that satisfy the stringent condition from Equation (6) or the relaxed condition of Equation (7). This then means that the discovery of novel low energy isomers is possible knowing that these 'missing' isomers should have hybrid topologies satisfying equation (6).

Generally, we see that the low lying energetic minima of W_n, n = 7-10 cannot be distinguished by the types and numbers of critical points, b (that includes b_{HB}), r, c and l, see Tables 1-4. Therefore, an attempt to separate the low lying energetic minima a closer inspection of all the negative (3,+3) MESP critical point*s* is used. Histograms of all the (3,+3) MESP critical point*s* are analyzed for four of the W_n, n = 10 clusters. The H2O-10-1 and H2O-10-2 clusters possess the highest energy rank order and for comparison; H2O-10-t5 and H2O-10-t12 that have rather lower energetic stability are provided, see Table 4 and Table S4. More importantly, all four of these W_{10} clusters possess an identical number of lone pairs (l) based on the cutoff value (-31 kcal/mol). The two most energetically stable H2O-10-1 and H2O-10-2, show only the numerically high valued *LCP*s and the remnant (3,+3) critical points, see Figure 6(a) and Figure 6(b). This implies that no hydrogen bond is malformed utilizing (3,+1) *CP* instead of (3,+3) *CP* on the oxygen atom of H_2O in the cluster. It reflects the existence of a better hydrogen bonding network within these clusters. A nearly continuous distribution of MESP values however, is seen in histogram*s* corresponding to the H2O-10-t5 and H2O-10-t12 clusters, see Figure 6(c) and Figure 6(d) respectively. This is consistent with the presence of many weak and malformed hydrogen-bonds formed through (3,+1) critical points, that do not proportionally add to their energetic stability. Thus, a weak hydrogen bonding network renders these clusters lower in the energy rank order.

The topographical analysis is used to distinguish the low lying energetic minima of a larger water cluster; W_n, n = 12 by performing calculations using a small basis-set such as 3-21G since the topographical features of QTAIM and the MESP

are not significantly affected by the change of level of theory and basis set choice. It is therefore expected that we can supplement the energetic information with this topological data to sort the water clusters at lower computational cost. Therefore, candidate W_n, n = 12 clusters are optimized at MP2/3-21G level of theory starting with initial structures generated from force-field methods. The topographical features of $\rho(\boldsymbol{r})$ and MESP are both examined at the same level of theory. The hybrid topologies, b_{HB} and numbers of lone pairs (l) as well as the energy values that can be used to identify more optimal geometries are provided in Table S6 of the Supplementary Materials. A cluster having a relatively lower value of b_{HB} than does the GM can also be energetically favored due to the absence of malformed hydrogen-bond *BCP*s. The top ranked W_n, n = 12 clusters on the basis of the MP2/3-21G energies, possess a maximization of b_{HB}, minimization of l and sparsely populated histograms, conversely, lower-ranked n = 12 clusters can however be observed to possess a wide distribution of MESP (3, +3) critical points, see Table S6. This behavior was also seen for the less energetically stable W_n, n = 10 clusters; H2O-10-t5 and H2O-10-t12. The MP2/3-21G optimized W_n, n = 12 cluster geometries are further used as initial structures for an MP2/aug-cc-pvDZ level optimization. The energetic properties of the W_n, n = 12 clusters possessing correctly formed hydrogen-bond *BCP*s remained top ranked with respect to the larger basis set calculations. Therefore, based on these topological characteristics, it is possible to identify the low lying molecular clusters by employing inexpensive quantum chemical calculations. This study of W_n, n = 12 clusters is a first exercise of applying the hybrid QTAIM MESP topology criteria, emerging from W_n, n = 7-10 investigation. It needs further exploration for larger W_n clusters.

V. CONCLUSIONS:

The present work introduces the idea of the hybrid-QTPD, based on a chemically intuitive relation between the critical points of scalar fields of total electronic charge density $\rho(\boldsymbol{r})$ and the molecular electrostatic potential (MESP) for water W_n, n = 7-10. The original QTAIM and the new hybrid-QTPDs have both been employed to study the varying tendency of the water clusters to achieve $2D_{QT}$ or $3D_{QT}$ geometries. Both analyses of the QTAIM and hybrid versions of the QTPD were found to be almost invariant to the level of theory and basis sets. The QTAIM QTPD analysis is completely general and can be applied to any molecule, metals[44], clusters or solids[13,14,45]. The hybrid-QTPD analysis however, is more applicable to clusters of molecules containing lone pairs and hydrogen-bonds, such as NH_3 and HCN. The energetically stable isomers display limited topological diversity by virtue of their integer solution sets that are bounded by 'forbidden' and 'unstable' regions in the respective solution space of both the QTAIM and hybrid-QTPDs. This shows that the energetically stable isomers of a given set of water clusters W_n, n = 7-10 are confined to a narrow zone in both types of QTPDs. This is in contrast to the unbounded diversity of the associated potential energy surface. The consideration of the Euler Characteristic χ = -1 may be useful for identifying features of 'missing' hybrid-QTPD topologies of the more energetically stable isomers.

It was observed that the position of the global minimum migrated from the lower bound D_L to the upper bound D_U of the QTPD with increase in water cluster size from W_n, n = 4-10. Using the new QTPD structure measure, D_L it was found that the QTPDs for n = 4, 5 can be characterized as different from the n = 6-10 QTPDs. This is consistent with the finding that the quantum dimensionalities of the global minimum for W_n, n = 4,5 are 2-D_{QT}, i.e. planar and those of the global minimum for n = 6-10 are all 3-D_{QT}, corresponding to compact topologies.

The findings from the analysis of the W_n, n = 6-10 QTPDs using the values of $H(\mathbf{r}_b) < 0$ of the hydrogen-bond *BCP*s and the hydrogen-bond *BCP* number density ($b_{HB}/2n$) are in agreement with earlier energetic based studies on n = 7-16 that found energetic stability increased due to the large number of hydrogen-bond *BCP*s for clusters with an even number of monomers.[44] Future work could provide insights from the topology into the previous energetic based findings that for W_n, n = 7-16, the energetic stability was found to increase due to a large number of hydrogen-bond *BCP*s for clusters with an even number of water monomers [4]. Also linked to the same investigation was the finding that for W_n, n = 17-30 the increase in energetic stability was found for clusters with an *odd* number of water monomers.

The hybrid-QTPDs constructed from a relation created between the number of oxygen lone pairs using the negative MESP (3,+3) critical points (l) and the hydrogen-bond *BCP*s (b_{HB}) from the QTAIM analysis. It was discovered that the topologies that obeyed inequality $b_{HB} + l > 2n$ always yielded more energetically unstable solutions than the subset defined by the relation, $b_{HB} + l = 2n$. This is because the combination of number of hydrogen-bonds and number of remaining lone pairs in water clusters plays a critical role in ensuring their energetic stability. It indeed turns out that certain of the water isomers containing more hydrogen-bond *BCP*s than the corresponding global minimum structure possess higher energy because of the larger number of lone pairs contained in them.

Histogram studies of the W_n, n = 10,12 of all the negative valued (3,+3) MESP critical point*s* further helps to explain the energetic stability of water clusters by the variation of the histogram distributions. From the histogram study of W_n, n = 10, it can be seen that the maximization of b_{HB} and presence of distinct and deep (3,+3) MESP critical point*s* l are useful initial criteria to select lower energy clusters. With this information we proceeded to undertake a study on the larger W_n, n = 12 clusters to test and then to confirm the feasibility in terms of computational cost.

The limited topological diversity of the local energy minima of both the QTAIM and hybrid-QTPDs is in contrast to their wide range of energetic diversities and indicates their use for sorting the local minima in terms of energetic rank orderings. Further to this, the insights gained from this study on W_n, n = 7-10 clusters have been used to sort and identify the topologically stable n = 12, clusters using quantum chemical calculations at very low level of theory. Therefore, it is hoped in future this hybrid-QTPD analysis will find extensive use for sorting any molecular clusters where lone pairs play crucial role in determining the structure.

CORRESPONDING AUTHORS:

Professor Samantha Jenkins
College of Chemistry and Chemical Engineering, Hunan Normal University
Changsha, Hunan 410081, China
Email: samanthajsuman@gmail.com

Professor Shridhar R. Gadre
Department of Chemistry,
I.I.T. Kanpur, Kanpur 208016, India
Email: gadre@iitk.ac.in

ACKNOWLEDGMENTS

A.K. thanks the Council of Scientific and Industrial Research (CSIR), New Delhi for a research fellowship. S.R.G. is thankful to the Department of Science and Technology (DST), New Delhi for financial support. The One Hundred Talents Foundation of Hunan Province and the aid program for the Science and Technology Innovative Research Team in Higher Educational Institutions of Hunan Province are gratefully acknowledged for the support of S. J. and S. R. K. The National Natural Science Foundation of China is also gratefully acknowledged, project approval number: 21273069.

REFERENCES:

1 S. Maheshwary, N. Patel, N. Sathyamurthy, A. D. Kulkarni and S. R. Gadre, *J. Phys. Chem. A*, 2001, **105**, 10525–10537.
2 J. Sadlej, V. Buch, J. K. Kazimirski and U. Buck, *J. Phys. Chem. A*, 1999, **103**, 4933–4947.
3 D. J. Wales and M. P. Hodges, *Chem. Phys. Lett.*, 1998, **286**, 65–72.
4 S. R. Gadre, S. D. Yeole and N. Sahu, *Chem. Rev.*, 2014, **114**, 12132–12173.
5 F. N. Keutsch and R. J. Saykally, *Proc. Natl. Acad. Sci.*, 2001, **98**, 10533–10540.
6 T. Miyake and M. Aida, *Chem. Phys. Lett.*, 2002, **363**, 106–110.
7 S. McDonald, L. Ojamäe and S. J. Singer, *J. Phys. Chem. A*, 1998, **102**, 2824–2832.
8 T. P. Radhakrishnan and W. C. Herndon, *J. Phys. Chem.*, 1991, **95**, 10609–10617.
9 S. Jenkins, *Int. J. Quantum Chem.*, 2013, **113**, 1603–1608.
10 S. Jenkins, A. Restrepo, J. David, D. Yin and S. R. Kirk, *Phys. Chem. Chem. Phys.*, 2011, **13**, 11644–11656.
11 S. Jenkins, C. Rong, S. R. Kirk, D. Yin and S. Liu, *J. Phys. Chem. A*, 2011, **115**, 12503–12511.
12 R. F. W. Bader, *Atoms in Molecules: A Quantum Theory*, Oxford University Press, USA, 1994.
13 S. Jenkins and I. Morrison, *Chem. Phys. Lett.*, 2000, **317**, 97–102.
14 S. Jenkins and I. Morrison, *J. Phys. Chem. B*, 1999, **103**, 11041–11049.
15 P. W. Ayers and S. Jenkins, *Comput. Theor. Chem.*
16 S. Jenkins, *J. Phys. Condens. Matter*, 2002, **14**, 10251–10263.
17 S. Jenkins, P. W. Ayers, S. R. Kirk, P. Mori-Sánchez and A. Martín Pendás, *Chem. Phys. Lett.*, 2009, **471**, 174–177.
18 M. J. Bearpark, F. Bernardi, M. Olivucci, M. A. Robb and B. R. Smith, *J. Am. Chem. Soc.*, 1996, **118**, 5254–5260.
19 W. L. Cao, C. Gatti, P. J. MacDougall and R. F. W. Bader, *Chem. Phys. Lett.*, 1987, **141**, 380–385.
20 R. F. W. Bader, *Acc. Chem. Res.*, 1975, **8**, 34–40.
21 K. Collard and G. G. Hall, *Int. J. Quantum Chem.*, 1977, **12**, 623–637.
22 C. K. Johnson, in *Abstracts of the American Crystallographic Association*, Asilomar, CA, 1977, p. 30.
23 V. H. Smith, P. F. Price and I. Absar, *Isr. J. Chem.*, 1977, **16**, 187–197.
24 D. Cremer and E. Kraka, *Croat. Chem. Acta*, 1984, **57**, 1265–1287.

25 E. D. Isaacs, A. Shukla, P. M. Platzman, D. R. Hamann, B. Barbiellini and C. A. Tulk, *Phys. Rev. Lett.*, 1999, **82**, 600–603.
26 S. R. Gadre, R. N. Shirsat and S. R. Garde, *Electrostatics of Atoms and Molecules*, Sangam Books Ltd, Hyderabad, 2001.
27 E. Scrocco and J. Tomasi, in *New Concepts II*, Springer Berlin Heidelberg, 1973, pp. 95–170.
28 A. Kumar, S. R. Gadre, N. Mohan and C. H. Suresh, *J. Phys. Chem. A*, 2013, **118**, 526–532.
29 S. R. Gadre and P. K. Bhadane, *J. Chem. Phys.*, 1997, **107**, 5625–5626.
30 M. M. Deshmukh, L. J. Bartolotti and S. R. Gadre, *J. Phys. Chem. A*, 2007, **112**, 312–321.
31 P. Politzer and J. S. Murray, *Theor. Chem. Acc.*, 2002, **108**, 134–142.
32 P. Politzer, J. S. Murray and T. Clark, *Phys. Chem. Chem. Phys.*, 2010, **12**, 7748–7757.
33 R. K. Pathak and S. R. Gadre, *J. Chem. Phys.*, 1990, **93**, 1770–1773.
34 M. Leboeuf, A. M. Köster, K. Jug and D. R. Salahub, *J. Chem. Phys.*, 1999, **111**, 4893–4905.
35 D. Roy, P. Balanarayan and S. R. Gadre, *J. Chem. Phys.*, 2008, **129**, 174103.
36 P. Balanarayan and S. R. Gadre, *J. Chem. Phys.*, 2003, **119**, 5037–5043.
37 C.-X. Xiao, T. Xu, J. R. Maza, F. A. Figueredo, S. R. Kirk and S. Jenkins, *Chem. Phys. Lett.*, 2014, **609**, 117–122.
38 J. R. Maza, S. Jenkins, S. R. Kirk, J. S. M. Anderson and P. W. Ayers, *Phys. Chem. Chem. Phys.*, 2013, **15**, 17823–17836.
39 S. D. Yeole and S. R. Gadre, *J. Chem. Phys.*, 2011, **134**, 084111.
40 R. M. Shields, B. Temelso, K. A. Archer, T. E. Morrell and G. C. Shields, *J. Phys. Chem. A*, 2010, **114**, 11725–11737.
41 T. A. Keith, *AIMAll*, TK Gristmill Software, Overland Park KS, USA, 2012.
42 S. D. Yeole, R. López and S. R. Gadre, *J. Chem. Phys.*, 2012, **137**, 074116.
43 J. F. Rico, R. López, I. Ema and G. Ramírez, *J. Comput. Chem.*, 2004, **25**, 1347–1354.
44 S. R. Gadre, S. D. Yeole and N. Sahu, *Chem. Rev.*, 2014, 141024082839008.
45 T. Xu, S. Jenkins, C.-X. Xiao, J. R. Maza and S. R. Kirk, *Chem. Phys. Lett.*, 2013, **590**, 41–45.
46 S. Jenkins, S. R. Kirk, A. S. Cote, D. K. Ross and I. Morrison, *Can. J. Phys.*, 2003, **81**, 225–231(7).

Figure 1. Molecular graphs of selected QTAIM topologies of W_n, n = 7-10 are shown in sub-figures (a)-(d) respectively. In addition to the global energy minimum indicated by (GM) for each of the W_n, n = 7-10 a selection of molecular graphs correspond to equal or higher topological complexity (Σ_{brc}). The bond (*BCP*), ring (*RCP*) and cage (*CCP*) critical point sets, are visible as unmarked green, red and blue spheres, respectively. Additionally, O---O *BCP* bond-paths are marked by dashed lines, e.g. shown in sub-figure (d) for H2O-10-t10, O7---O27, see also Tables 1-4, see section **II(i)** for further details.

Figure 2. The total electronic charge density $\rho(\mathbf{r})$ quantum topology phase diagrams (QTPDs) of water clusters W_n, n = 7-10 are presented in sub-figures (a)-(d) respectively. The topology corresponding to GM represents the global energy minimum. Note that for W_n, n = 7 the estimated upper boundary of the QTPD (26,7) and for W_n, n = 9 the estimated upper boundary of the QTPD (32,7), see Table 5, section **II(iii)** and section **IV(i)** for further details.

Figure 3. The variations of $H(\mathbf{r}_b)$ with bond-path length (BPL) for the W_n, n = 7-10 molecular graphs are presented in sub-figures (a)-(d) respectively. A degree of covalent bond character and hence cooperative effects is present for the local total energy density $H(\mathbf{r}_b) < 0$. Conversely, values of $H(\mathbf{r}_b) > 0$ indicate no covalent bond character and a lack of cooperative effects and hence weaker hydrogen-bond *BCP*s, see Figure 1(a-d), all entities are in a.u.

Figure 4. Structures of the molecular electrostatic potential (MESP) topologies corresponding to the QTAIM equivalents in Figure 1 are given in sub-Figures (a-d). The MESP hydrogen-bond *BCP*s and the negative MESP (3,+3) *LCP*s are denoted by grey and red spheres respectively, see section **II(ii)** for further details. In sub-figure (a) and (d) the black arrows indicate the oxygen atom where weak ($H(\mathbf{r}_b) > 0$) hydrogen-bond *BCP*s are formed, see section **IV(ii)** for further details.

Figure 5. Hybrid-QTPDs quantum topology phase diagrams (QTPDs) of the W_n, n = 7-10 water clusters are presented in sub-figures (a)-(d) respectively. The Euler characteristic $\chi = 0$ unless otherwise specified on the sub-figures. The black line at the boundary of the 'forbidden' and 'stable' regions represents the solutions of the relation, $b_{HB} + l = 2n$, see section **IV(ii)** for further details.

Figure 6. Histograms for four W_n, n = 10 geometries (a) H2O-10-1, (b) H2O-10-2, (c) H2O-10-t5 and (d) H2O-10-t12. The x-axis of histogram represents the magnitude of MESP values at (3,+3) critical points and the y-axis represents their count. See the main text for further details.

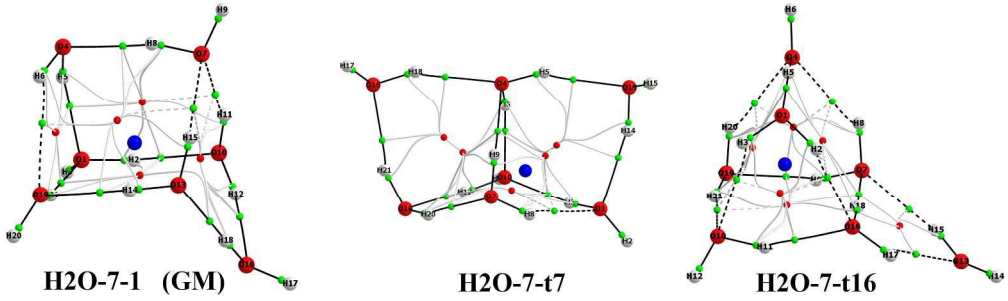

Figure 1(a). Molecular graphs of the W_n, *n = 7, QTAIM topology. In addition to the global energy minimum indicated by (GM) a selection of molecular graphs correspond to equal or higher topological complexity (Σ_{brc}). The bond (BCP<), ring (RCP) and cage (CCP) critical point sets, are visible as unmarked green, red and blue spheres, respectively, see also Tables 1-4 and section II(i) for further details.*
958x278mm (72 x 72 DPI)

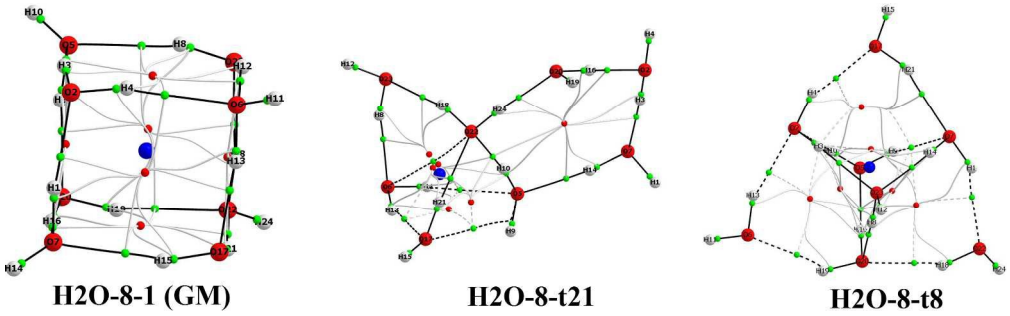

Figure 1(b). Molecular graphs of the W_n, *n = 8, QTAIM topology. See the caption of sub-figure 1(a) for further details.*
905x278mm (72 x 72 DPI)

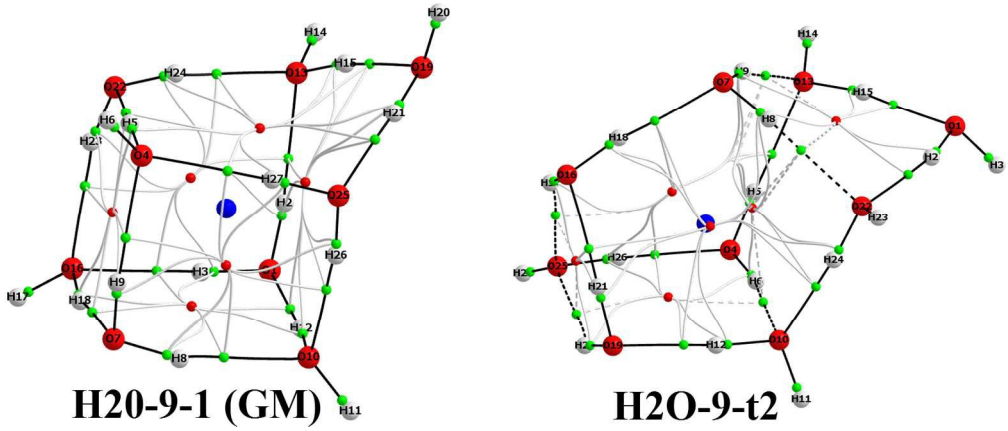

Figure 1(c). Molecular graphs of the W_n, *n = 9, QTAIM topology. See the caption of sub-figure 1(a) for further details.*
617x261mm (72 x 72 DPI)

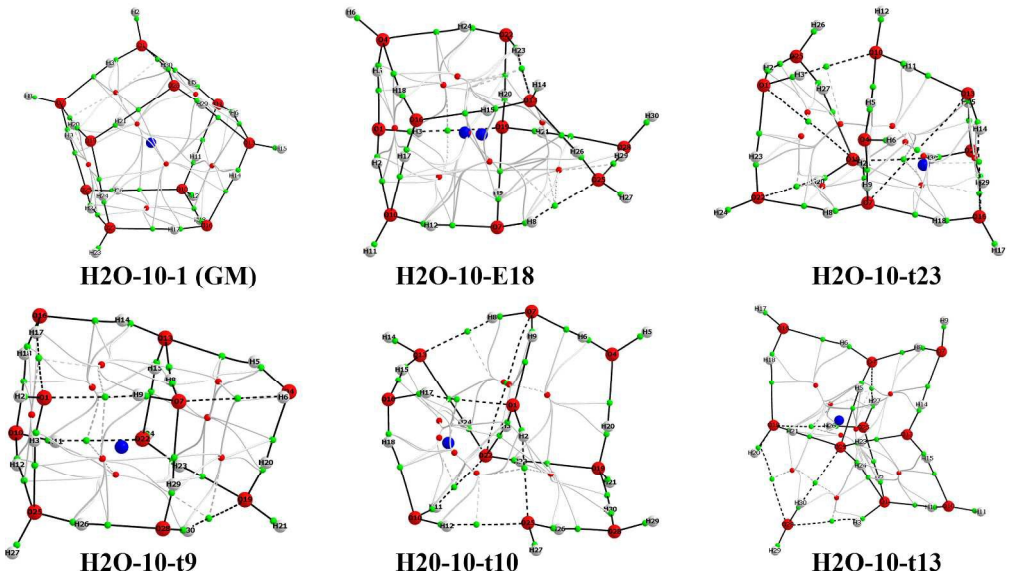

Figure 1(d). Molecular graphs of the W_n, *n = 10, QTAIM topology. Additionally, O---O BCP< bond-paths are marked by dashed lines for H2O-10-t10, O7---O27. See the caption of sub-figure 1(a) for further details. 984x558mm (72 x 72 DPI)*

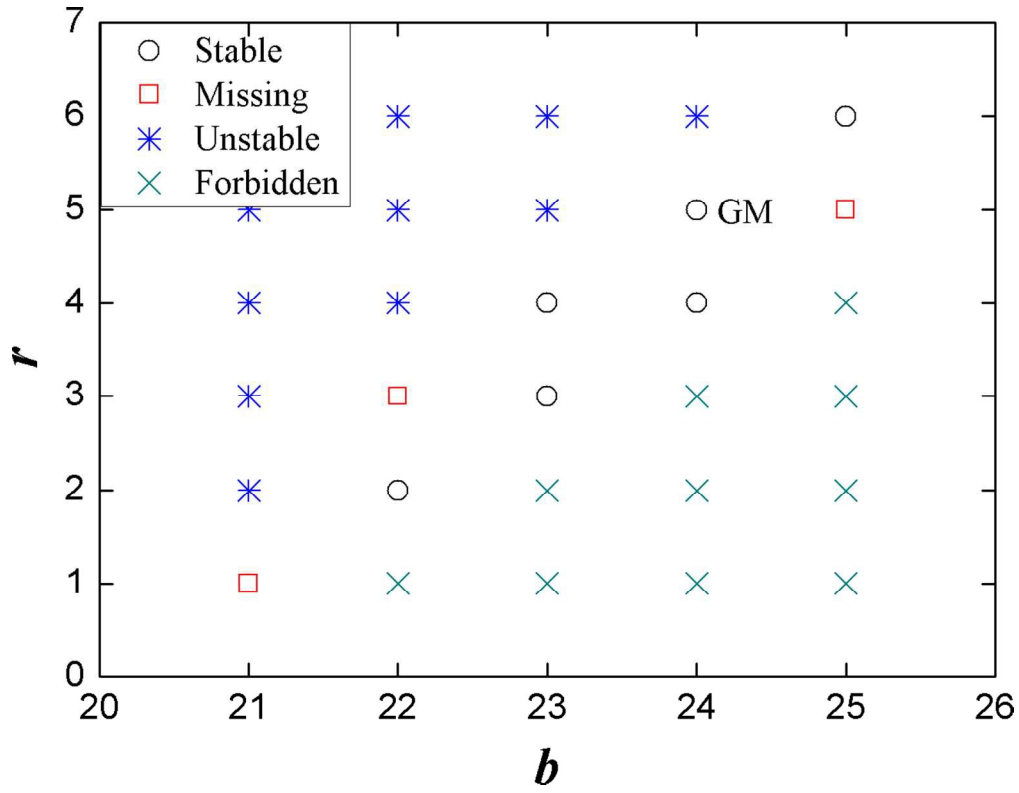

Figure 2(a). The QTAIM quantum topology phase diagram (QTPD) of the W_n, *n = 7 water cluster is presented. The topology corresponding to GM represents the global energy minimum. Note that for* W_7 *the estimated upper limit of the QTPD is at (26,7), see Table 5, section II(iii) and section IV(i) for further details.*

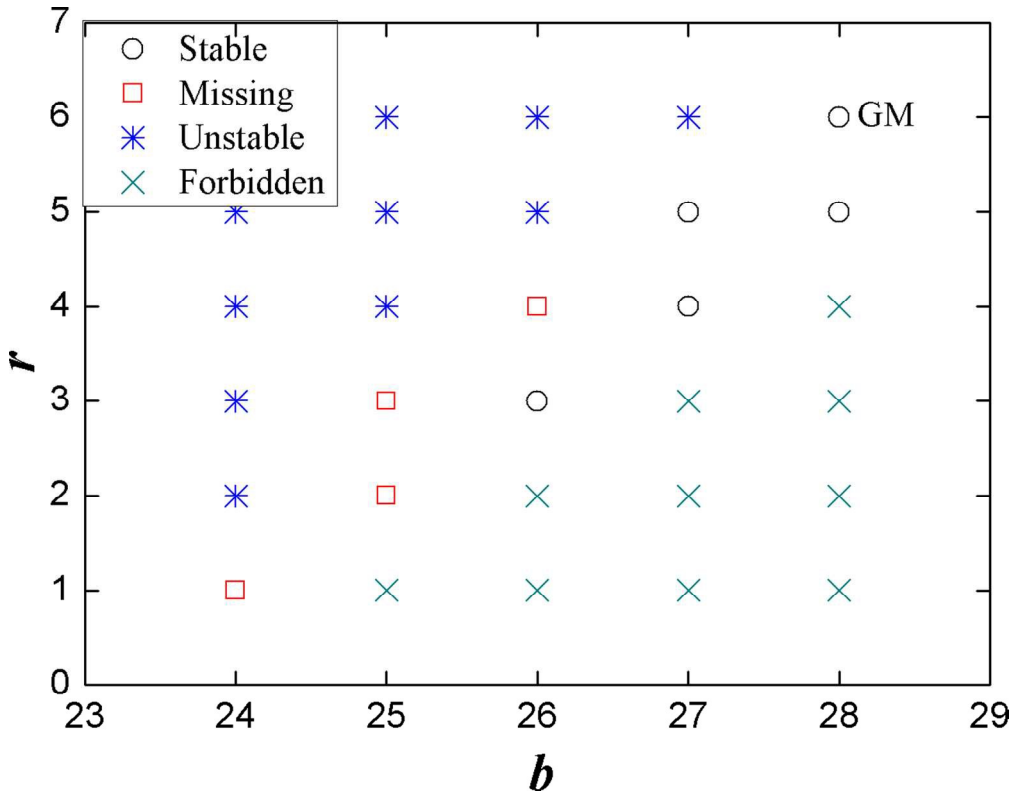

Figure 2(b). The QTAIM quantum topology phase diagram (QTPD) of the W_n, *n = 8 water cluster is presented, see the caption of Figure 2(a) for further details.*

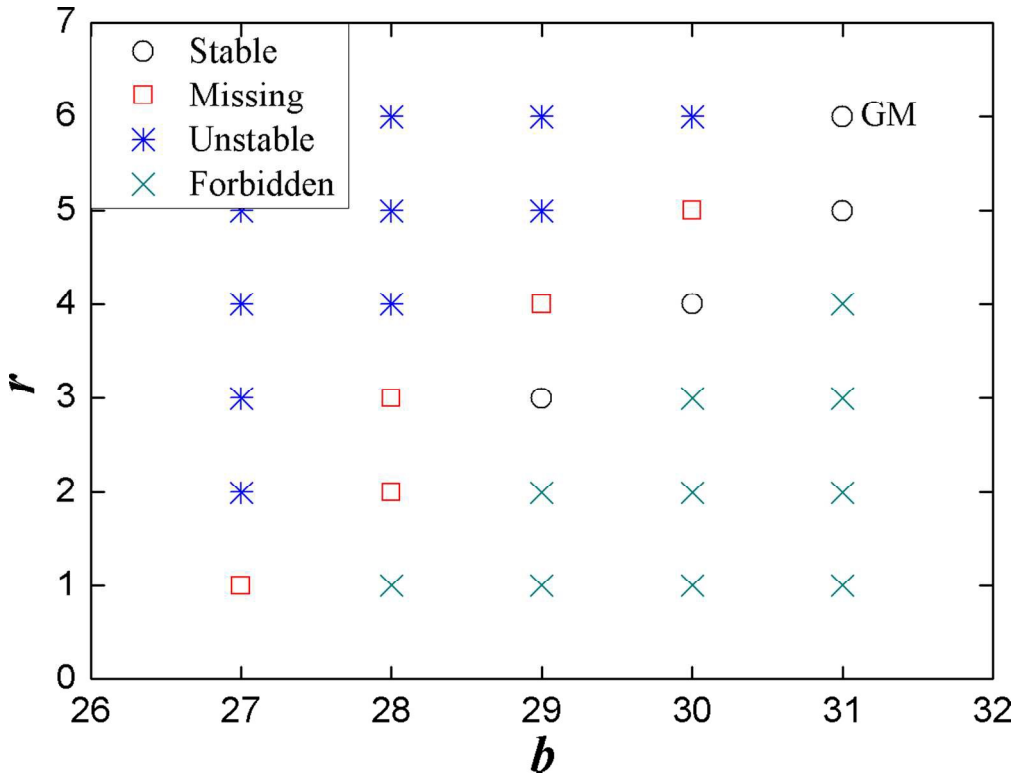

Figure 2(c). The QTAIM quantum topology phase diagram (QTPD) of the W_n, *n = 9 water cluster is presented, for* W_9 *the estimated upper limit of the QTPD is at (32,7), see the caption of Figure 2(a) for further details.*

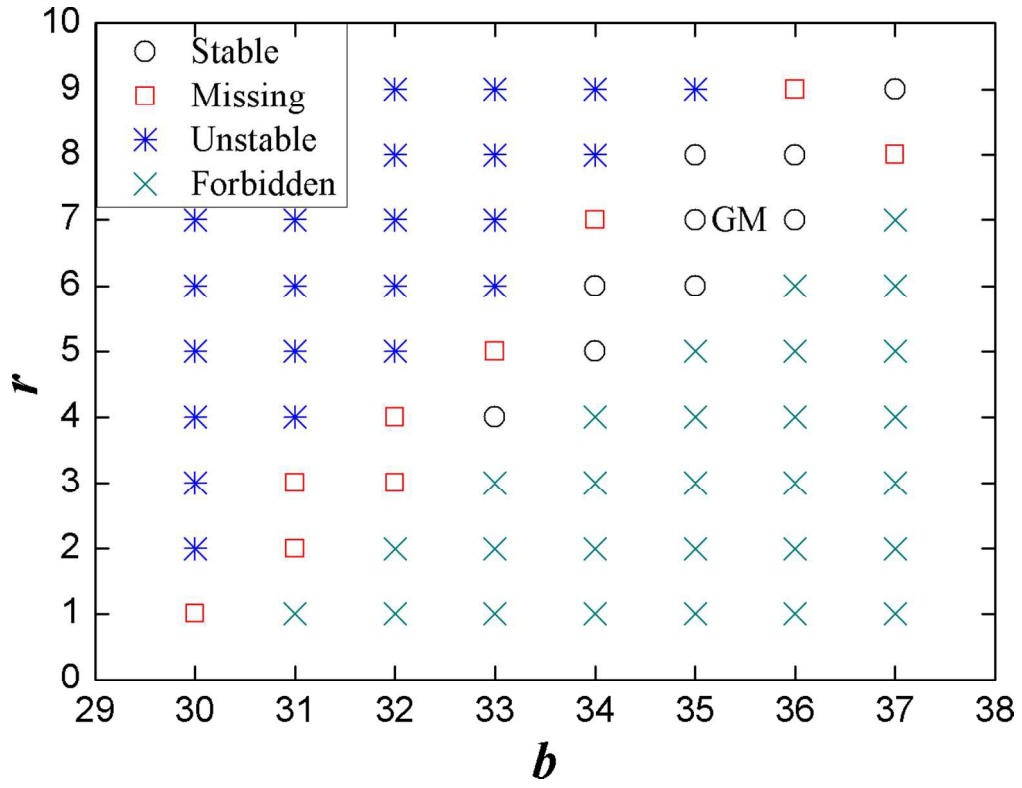

Figure 2(d). The QTAIM quantum topology phase diagram (QTPD) of the W_n, *n = 10 water cluster is presented, see the caption of Figure 2(a) for further details.*

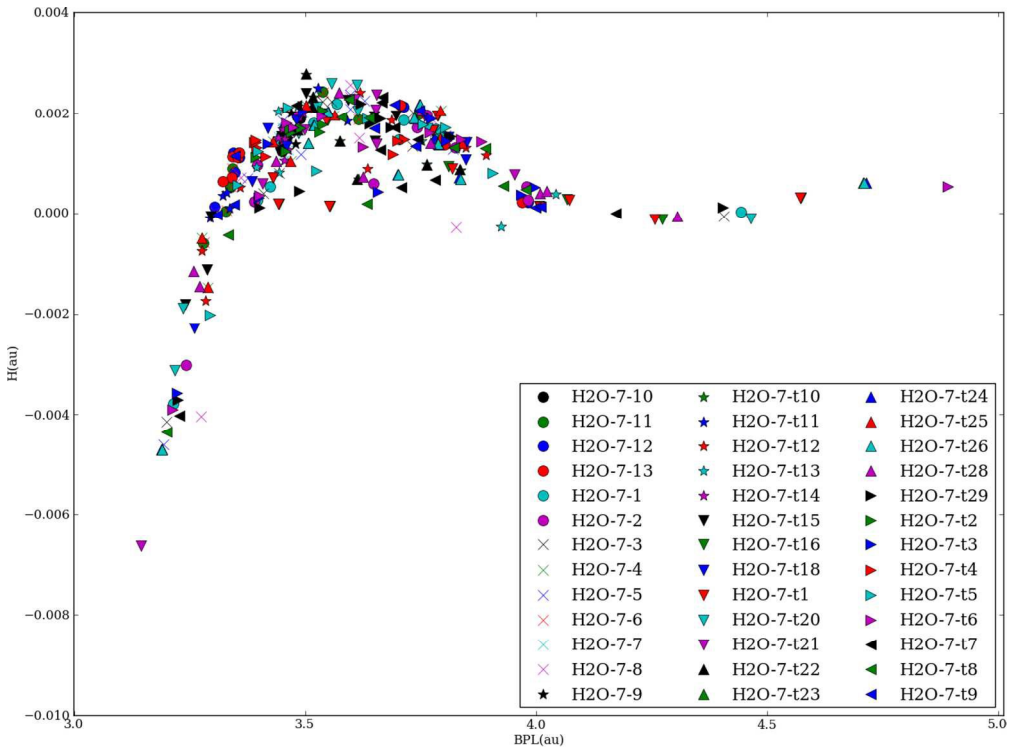

Figure 3(a). The variations of $H(\boldsymbol{r}_b)$ with bond-path length (BPL) for the molecular graph of the W_n, *n = 7 water cluster is presented. A degree of covalent bond character and hence cooperative effects is present for the local total energy density H(rb) < 0. Conversely, values of* $H(\boldsymbol{r}_b) > 0$ *indicate no covalent bond character and a lack of cooperative effects and hence weaker hydrogen-bond BCPs, see Figure 1(a-d), all entities are in a.u.*

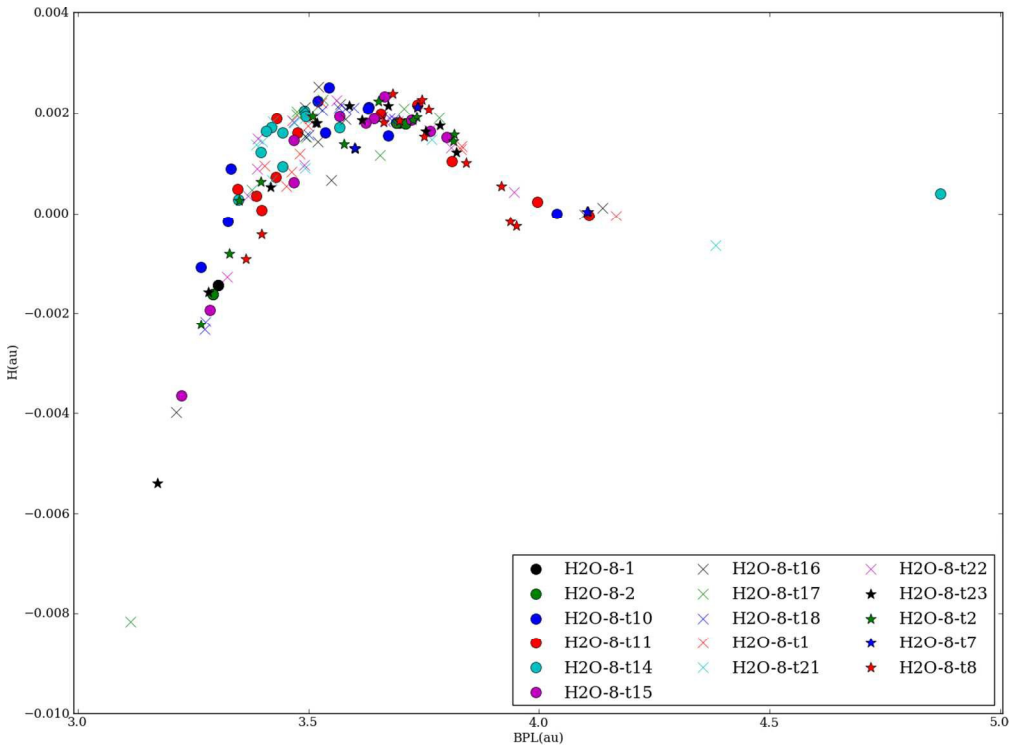

Figure 3(b). The variations of $H(\boldsymbol{r}_b)$ with bond-path length (BPL) for the molecular graph of the W_n, *n = 8 water cluster is presented, see the caption of Figure 3(a) for further details.*

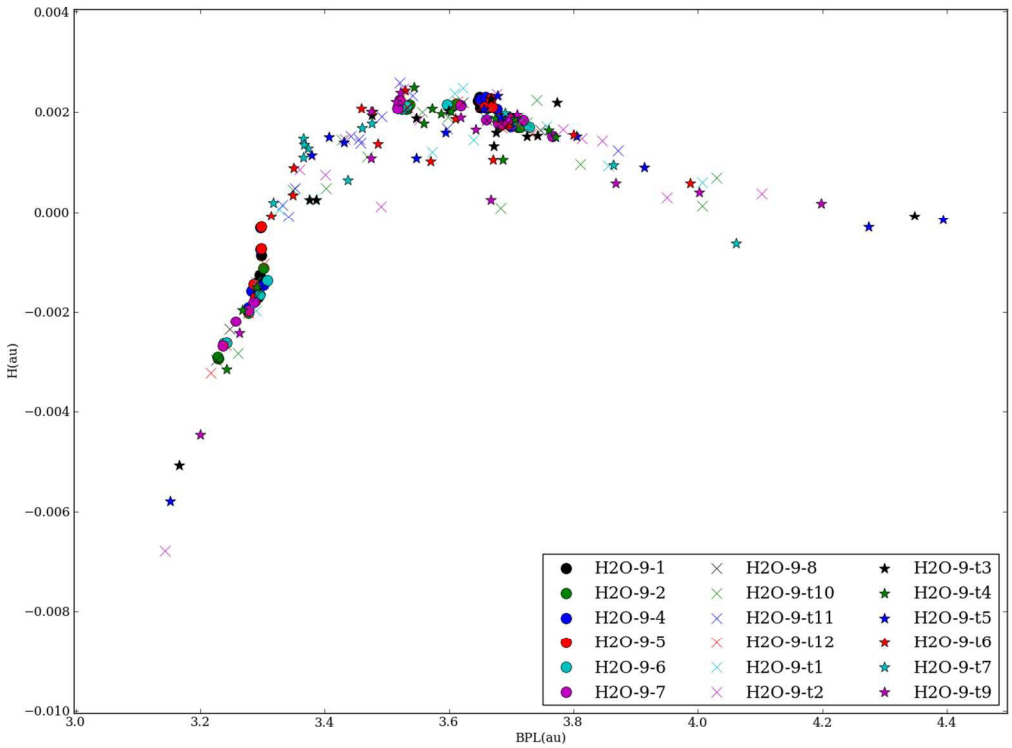

Figure 3(c). The variations of $H(\boldsymbol{r}_b)$ with bond-path length (BPL) for the molecular graph of the W_n, *n = 9 water cluster is presented, see the caption of Figure 3(a) for further details.*

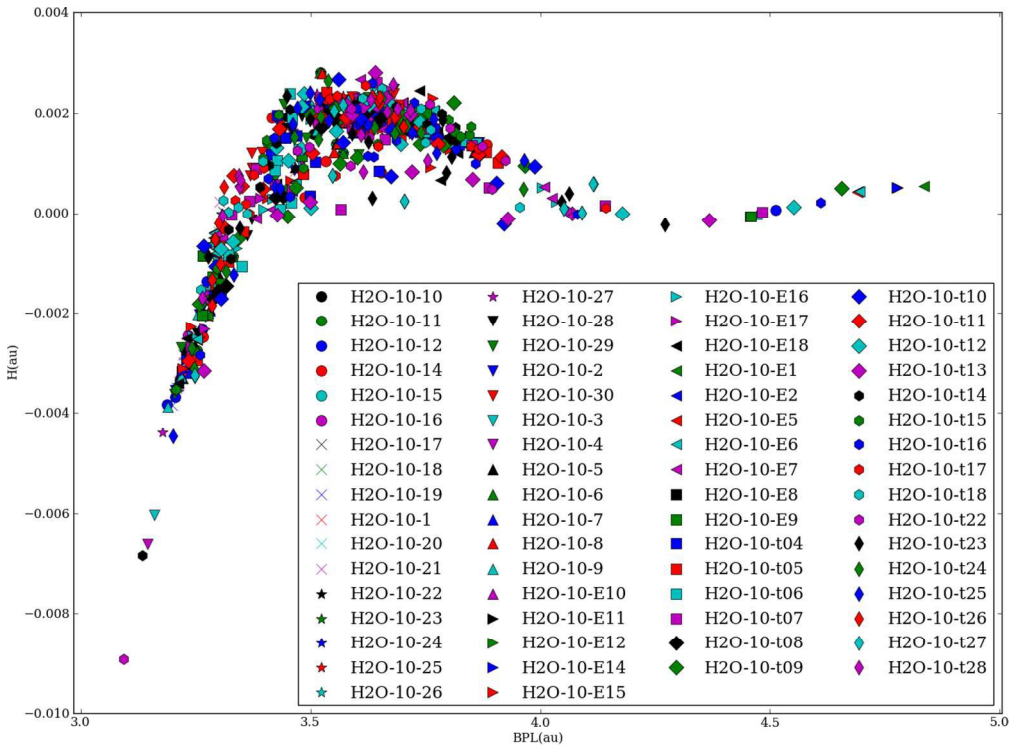

Figure 3(d). The variations of $H(\boldsymbol{r}_b)$ with bond-path length (BPL) for the molecular graph of the W_n, *n = 10 water cluster is presented, see the caption of Figure 3(a) for further details.*

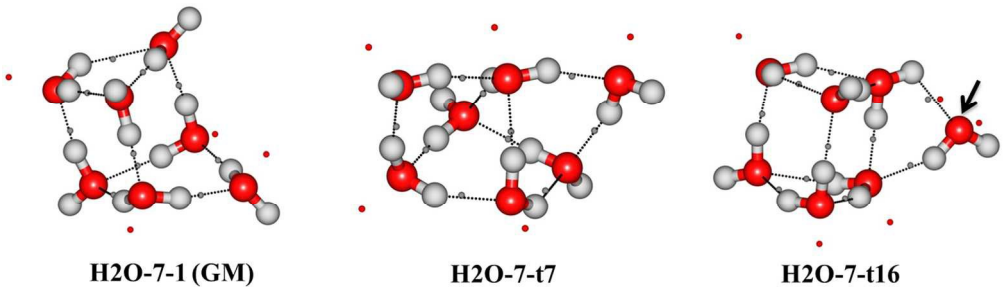

Figure 4(a). The structures of the molecular electrostatic potential (MESP) topologies for the W_n, *n = 7 water cluster is presented and the corresponding QTAIM equivalents in given Figure 1(a). The MESP hydrogen-bond BCPs and the MESP (3,+3) LCPs are denoted by grey and red spheres respectively, see section II(ii) for further details. The black arrow indicates the oxygen atom where weak (*$H(\mathbf{r}_b) > 0$*) hydrogen-bond BCPs are formed, see section IV(ii) for further details.*
247x74mm (150 x 150 DPI)

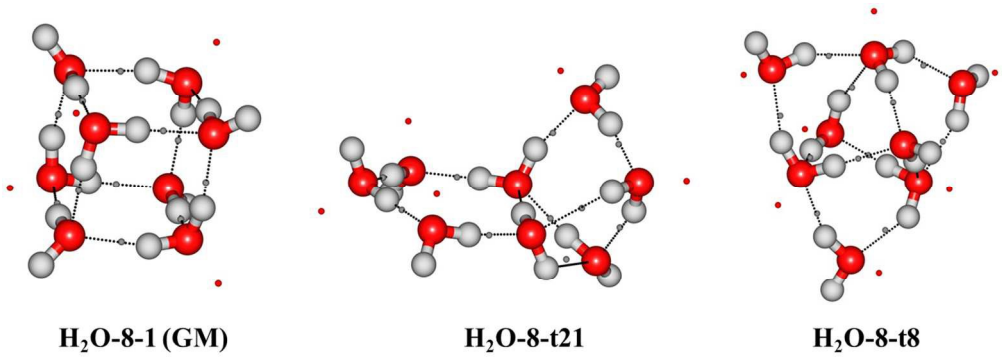

Figure 4(b). The structures of the molecular electrostatic potential (MESP) topologies for the W_n, *n = 8 water cluster is presented and the corresponding QTAIM equivalents in given Figure 1(b), see the caption of Figure 4(a) for further details.*
234x85mm (150 x 150 DPI)

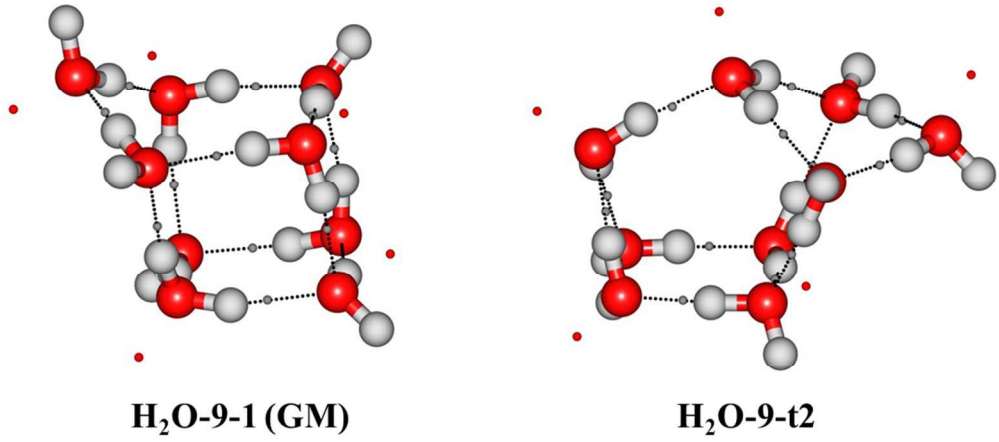

Figure 4(c). The structures of the molecular electrostatic potential (MESP) topologies for the W_n, *n = 9 water cluster is presented and the corresponding QTAIM equivalents in given Figure 1(c), see the caption of Figure 4(a) for further details.*
181x83mm (150 x 150 DPI)

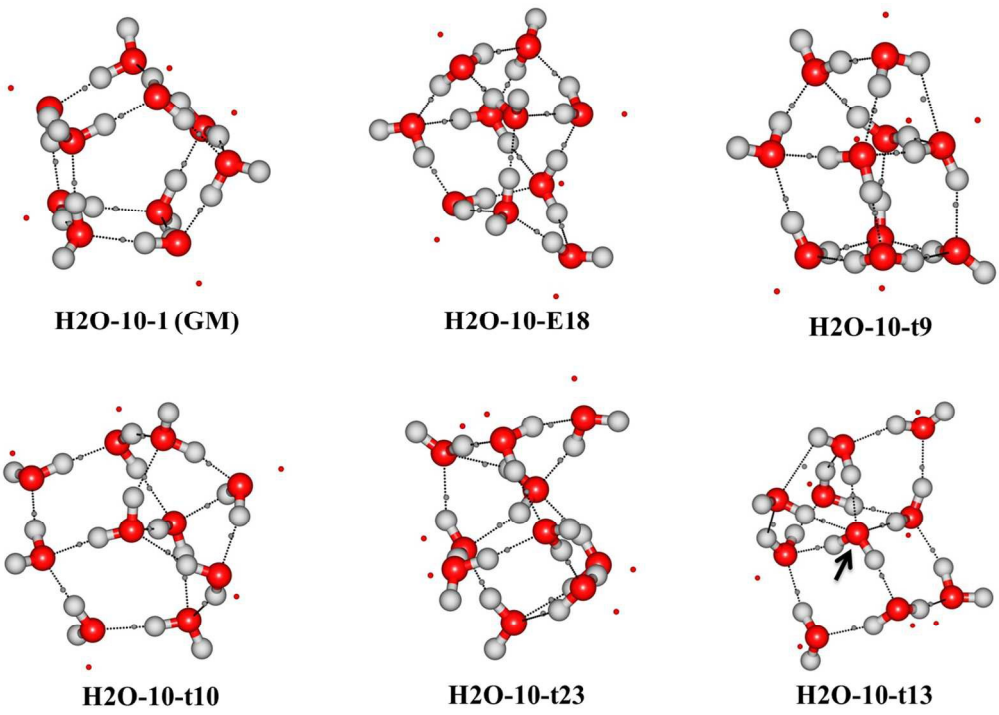

Figure 4(d). The structures of the molecular electrostatic potential (MESP) topologies for the W_n, *n = 10 water cluster is presented and the corresponding QTAIM equivalents in given Figure 1(d). The black arrow indicates the oxygen atom where weak (H(**r**$_b$) > 0) hydrogen-bond BCPs are formed, see the caption of Figure 4(a) for further details.*
237x172mm (150 x 150 DPI)

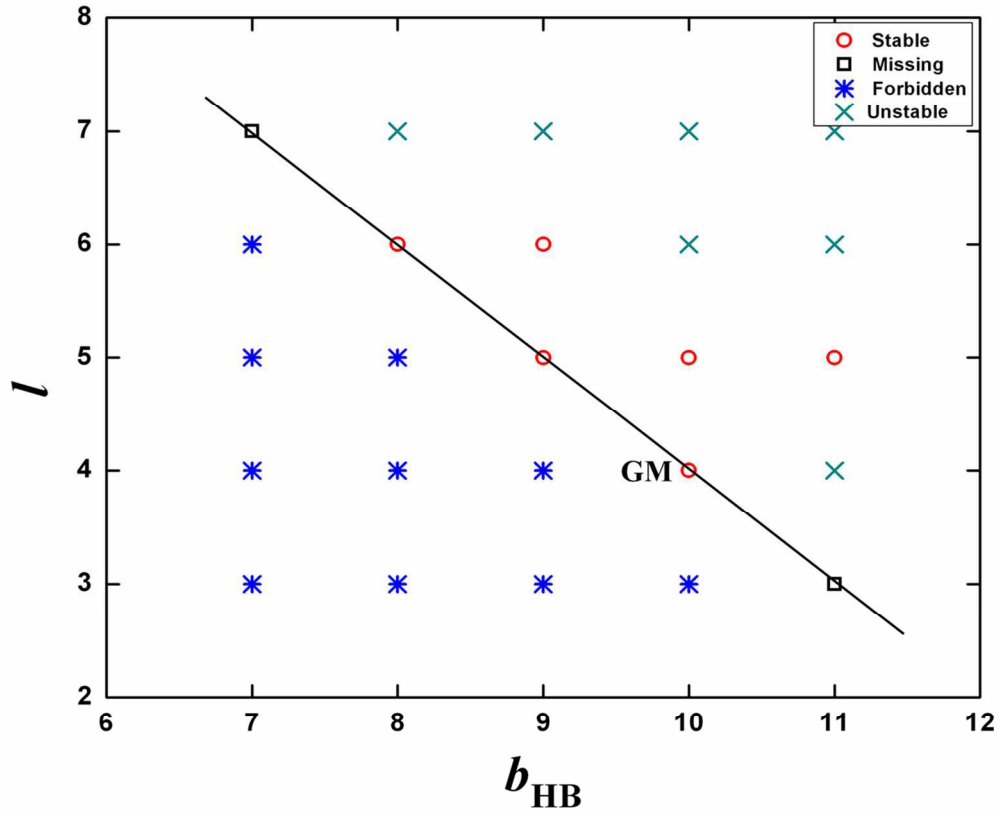

Figure 5(a). The hybrid-QTPD quantum topology phase diagram (QTPD) for the W_n, *n = 7 water cluster. The Euler characteristic χ = 0 unless otherwise specified on the sub-figures. The black line at the boundary of the 'forbidden' and 'stable' regions represents the solutions of the relation, bHB + l = 2n, see section IV(ii) for further details.*
214x174mm (150 x 150 DPI)

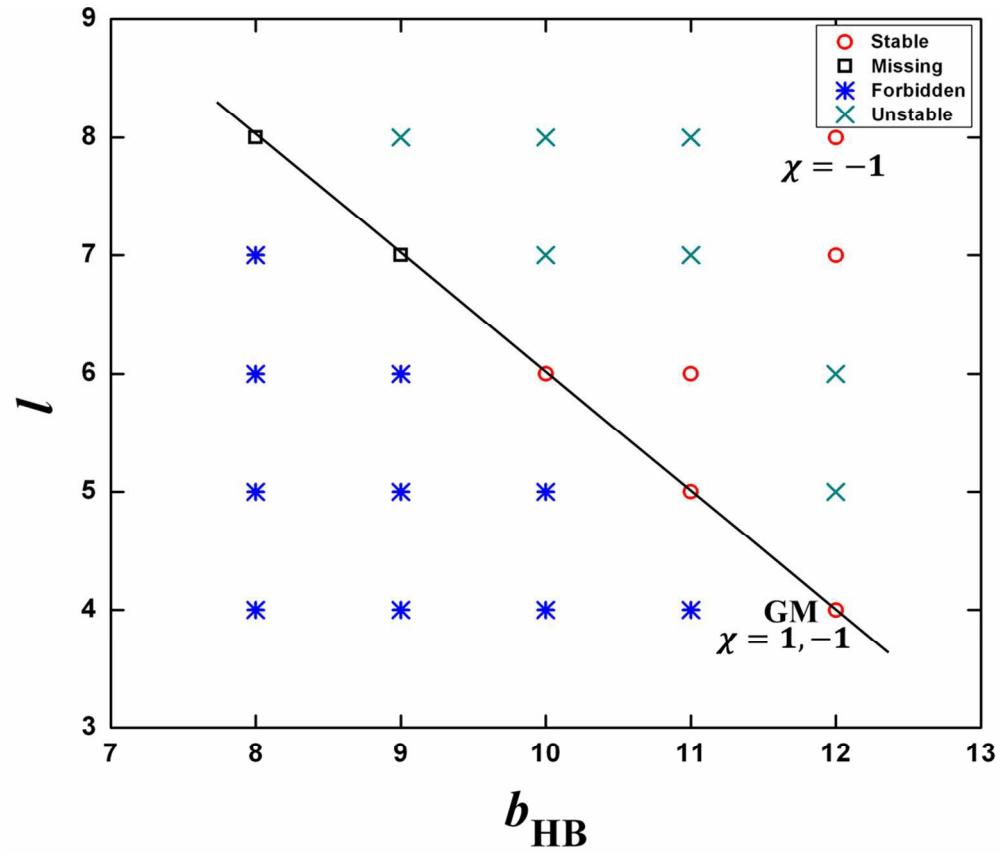

Figure 5(b). The hybrid-QTPD quantum topology phase diagram (QTPD) for the W_n, *n = 8 water cluster, see the caption of Figure 5(a) for further details.*
202x170mm (150 x 150 DPI)

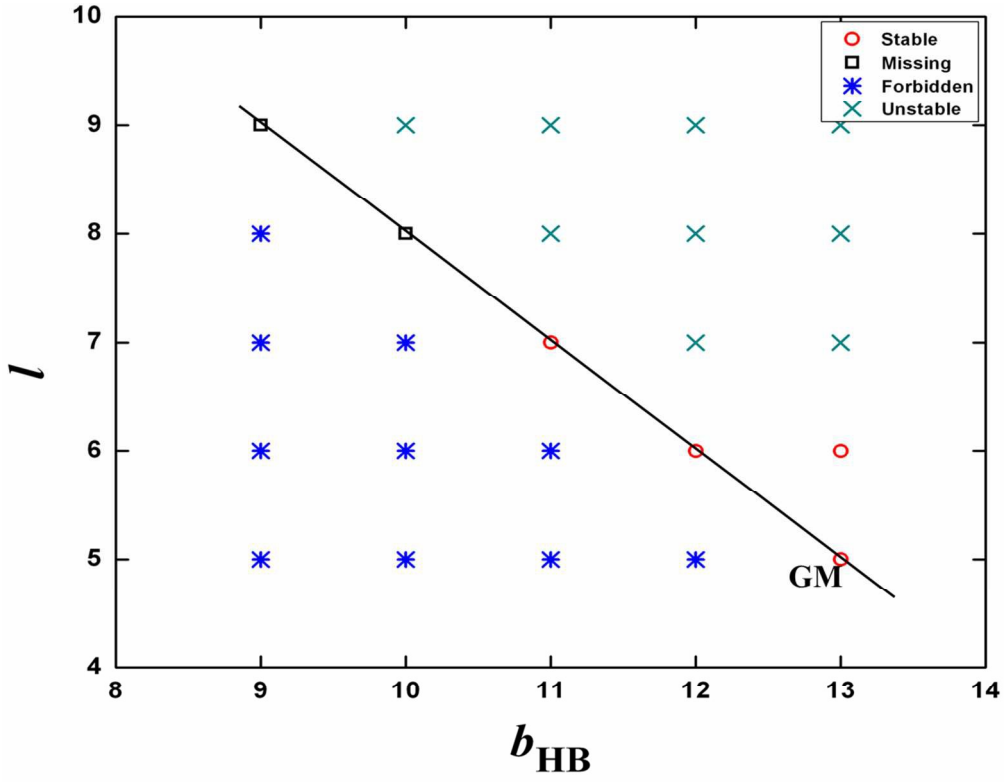

Figure 5(c). The hybrid-QTPD quantum topology phase diagram (QTPD) for the W_n, *n = 9 water cluster, see the caption of Figure 5(a) for further details.*
205x159mm (150 x 150 DPI)

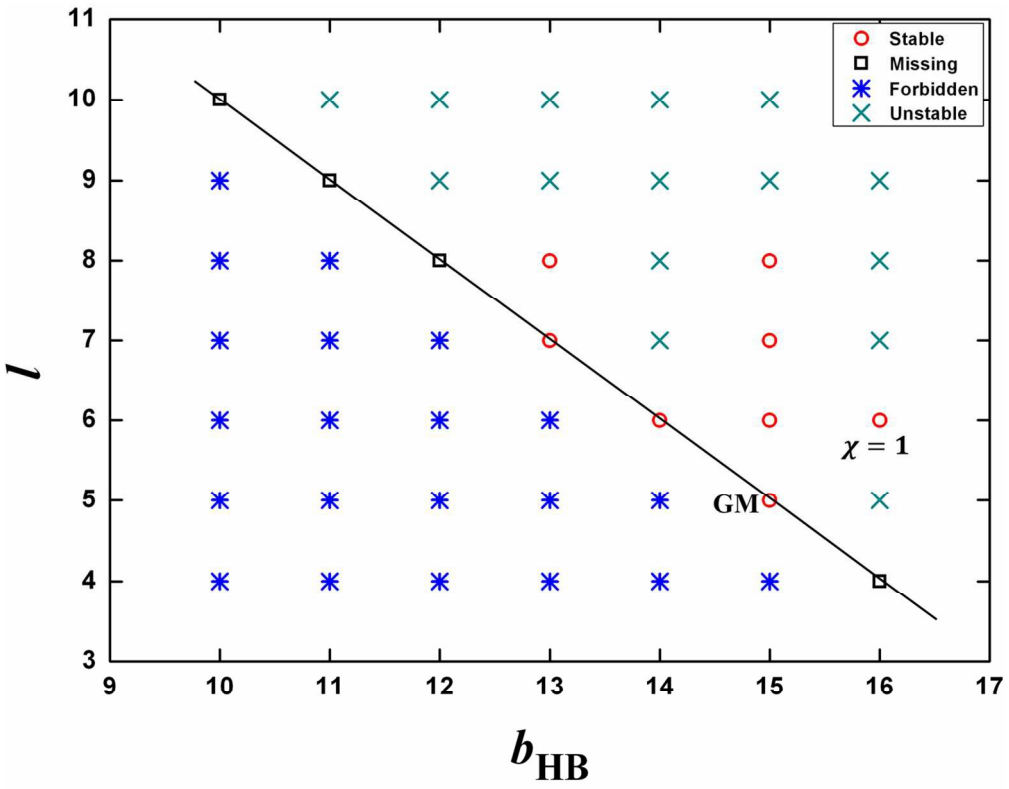

Figure 5(d). The hybrid-QTPD quantum topology phase diagram (QTPD) for the W_n, *n = 10 water cluster, see the caption of Figure 5(a) for further details.*
239x188mm (150 x 150 DPI)

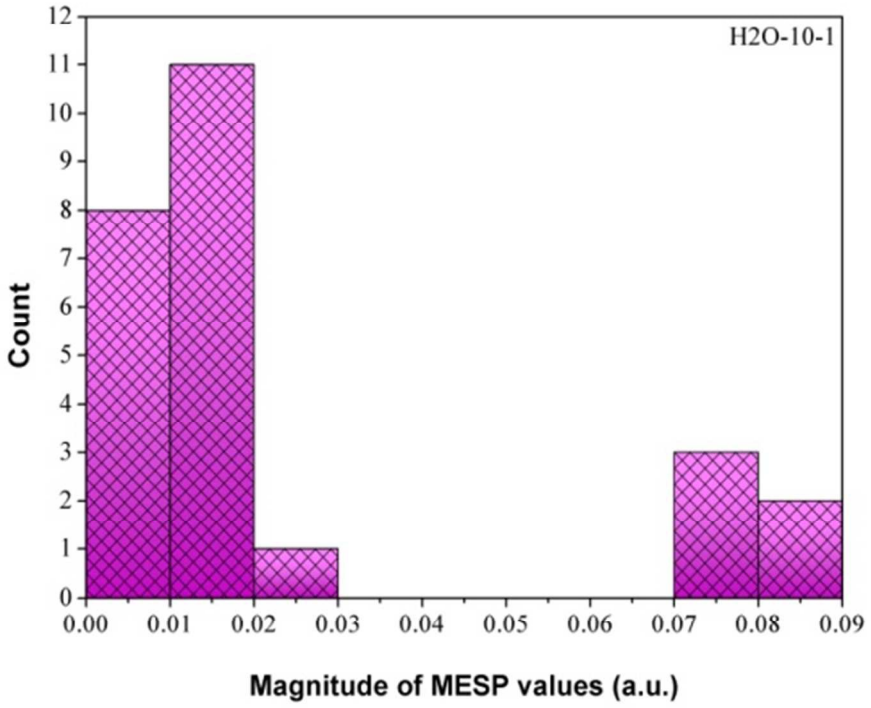

Figure 6(a). Histograms for the H2O-10-1 geometry of W_n, *n = 10. The x-axis of histogram represents the magnitude of MESP values at (3,+3) critical points and the y-axis represents their count, see the main text for further details.*

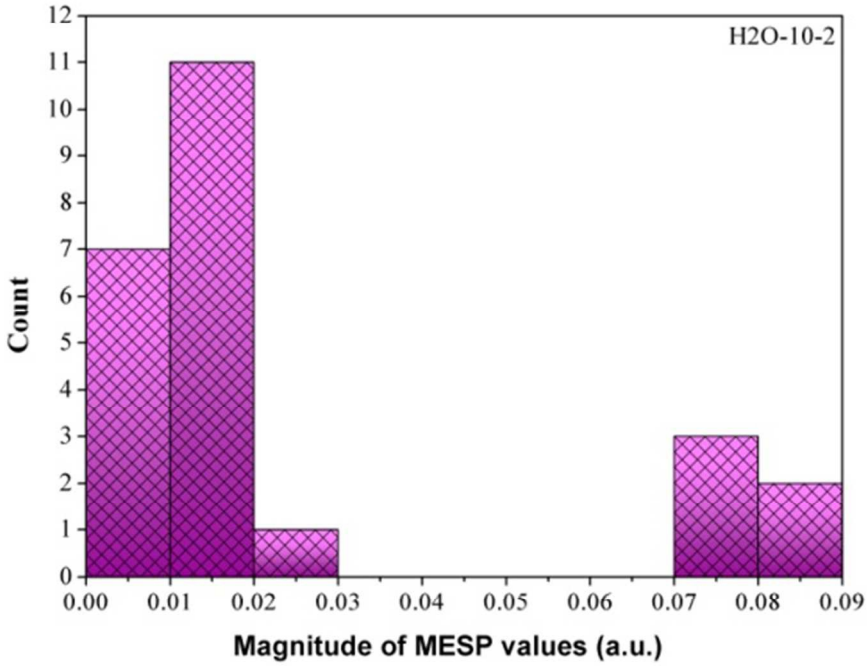

Figure 6(b). Histograms for the H2O-10-2 geometry of W_n, *n = 10, see the caption of Figure 6(a) for further details.*

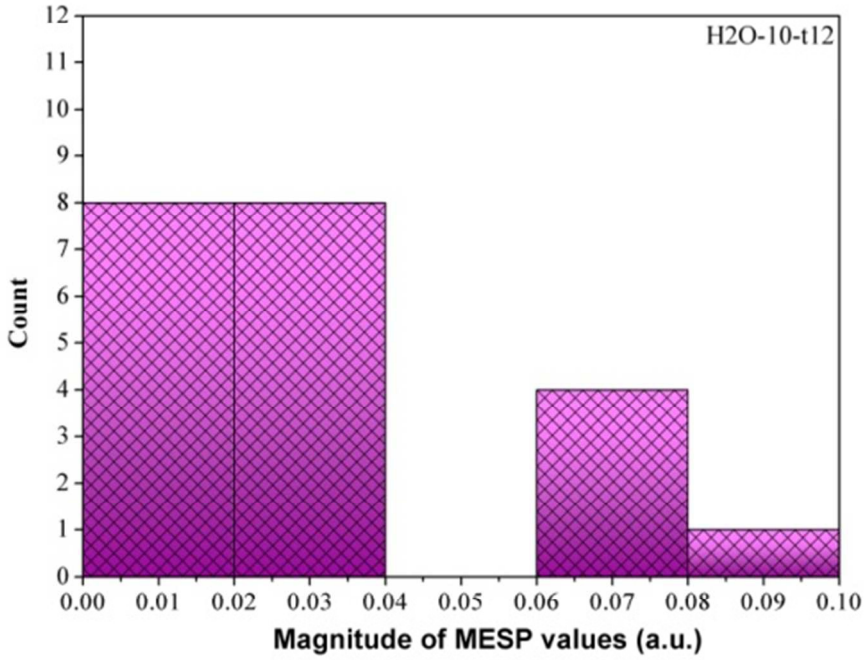

Figure 6(c). Histograms for the H2O-10-t5 geometry of W_n, *n = 10, see the caption of Figure 6(a) for further details.*

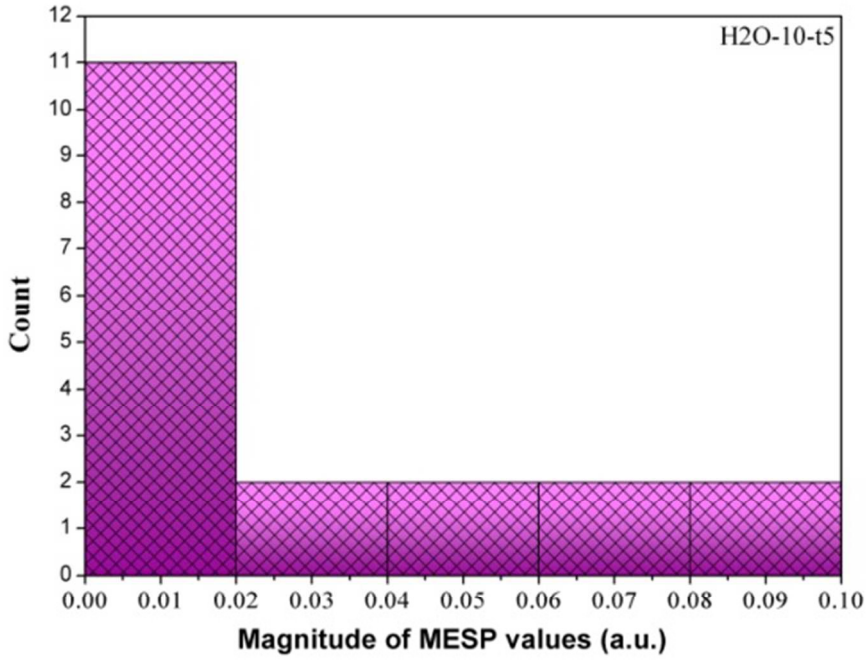

Figure 6(d). Histograms for the H2O-10-t12 geometry of W_n, *n = 10, see the caption of Figure 6(a) for further details.*

Table 1. A selection of the critical point data for the four varying sets of critical points for the isomeric QTPDs of the heptamer molecular graphs W_n, $n = 7$. The complete list of critical point data can be found in the Supplementary Materials Tables S1-S4. The numbers of QTAIM bond, ring and cage critical points are denoted by *b*, *r* and *c* respectively. The total number of *BCP*s is denoted *b* this includes the O-H sigma, H--O and O---O *BCP*s. The number of QTAIM hydrogen-bond *BCP*s are denoted by b_{HB}. The MESP critical points, the number of negative (3,+3) *LCP* critical points corresponding to the oxygen lone pairs are denoted by *l*. The bracketed values of *b* indicate the numbers of O---O *BCPs*. The topological complexity is denoted by the sum of the numbers of bond, ring and cage critical points; $\sum_{brc.}$ The relative energy ΔE is listed in a.u, all the structures were optimized at the MP2/aug-cc-pvDZ level.

Molecular Graph	*b*	b_{HB}	*r*	*c*	*l*	$\sum_{brc}$	ΔE
H2O-7-1	24	10	5	1	4	30	0
H2O-7-2	24	10	4	0	4	28	0.0007
H2O-7-3	24	10	5	1	4	30	0.0010
H2O-7-t3	24	10	4	0	4	28	0.0018
H2O-7-t8	24	10	5	1	4	30	0.0024
H2O-7-4	23	9	3	0	5	26	0.0028
H2O-7-t29	24	10	4	0	4	28	0.0031
H2O-7-t18	23	9	3	0	5	26	0.0034
H2O-7-t5	24(1)	9	4	0	5	28	0.0039
H2O-7-t12	23	9	3	0	5	26	0.0040
H2O-7-t28	24	10	4	0	4	28	0.0043
H2O-7-t7	24	10	5	1	5	30	0.0047
H2O-7-t11	22	8	2	0	6	24	0.0058
H2O-7-t20	23	9	4	1	5	28	0.0060
H2O-7-t23	24	10	4	0	5	28	0.0060
H2O-7-t15	23(1)	8	3	0	6	26	0.0060
H2O-7-t16	25	11	6	1	5	32	0.0062
H2O-7-t2	23	9	3	0	5	26	0.0062
H2O-7-11	22	8	2	0	6	24	0.0064
H2O-7-t10	23	9	3	0	6	26	0.0074
H2O-7-13	22	8	2	0	6	24	0.0096
H2O-7-t4	22	8	2	0	6	24	0.0105

Table 2. Critical point data for the isomeric QTPDs of the octamer molecular graphs W_n, n = 8. See the caption of Table 1 for further details.

Molecular Graph	*b*	b_{HB}	*r*	c	*l*	$\sum_{brc}$	ΔE
H2O-8-1	28	12	6	1	4	35	0
H2O-8-2	28	12	6	1	4	35	3E-05
H2O-8-t23	27	11	5	1	5	33	0.0088
H2O-8-t2	27	11	5	1	5	33	0.0089
H2O-8-t15	27	11	5	1	5	33	0.0098
H2O-8-t22	28(1)	11	5	0	5	33	0.0106
H2O-8-t1	27	11	4	0	6	31	0.0131
H2O-8-t11	27	11	4	0	6	31	0.0134
H2O-8-t16	27	11	4	0	5	31	0.0147
H2O-8-t17	26	10	3	0	6	29	0.0147
H2O-8-t18	26	10	3	0	6	29	0.0159
H2O-8-t21	28(2)	10	6	1	6	35	0.0161
H2O-8-t14	26	10	3	0	6	29	0.0165
H2O-8-t8	28	12	6	1	7	35	0.0178
H2O-8-t10	26	10	3	0	6	29	0.0180
H2O-8-t7	28	12	5	0	8	33	0.0244

Table 3. Critical point data for the isomeric QTPDs of the nonamer molecular graphs W_n, n =9. See the caption of Table 1 for further details.

Molecular Graph	*b*	b_{HB}	*r*	*c*	*l*	$\sum_{brc}$	ΔE
H2O-9-1	31	13	6	1	5	38	0
H2O-9-2	31	13	6	1	5	38	0.0004
H2O-9-4	31	13	6	1	5	38	0.0006
H2O-9-7	31	13	6	1	5	38	0.0009
H2O-9-8	31	13	6	1	5	38	0.0012
H2O-9-t4	31	13	6	1	5	38	0.0042
H2O-9-t1	31	13	5	0	6	36	0.0082
H2O-9-t10	31	13	6	1	5	38	0.0107
H2O-9-t9	31	13	5	0	5	36	0.0110
H2O-9-t2	31	13	6	1	5	38	0.0112
H2O-9-t3	31	13	5	0	5	36	0.0113
H2O-9-t6	30	12	4	0	6	34	0.0133
H2O-9-t5	31	13	5	0	6	36	0.0163
H2O-9-t11	29	11	3	0	7	32	0.0177
H2O-9-t7	29	11	3	0	7	32	0.0194

Table 4. Critical point data for the isomeric QTPDs of the decamer molecular graphs W_n, n =10. See the caption of Table 1 for further details.

Molecular Graph	b	b_{HB}	r	c	l	$\sum_{brc}$	ΔE
H2O-10-1	35	15	7	1	5	43	0
H2O-10-2	35	15	7	1	5	43	0.0002
H2O-10-3	35	15	7	1	5	43	0.0011
H2O-10-6	35	15	7	1	5	43	0.0025
H2O-10-t8	35	15	7	1	5	43	0.0033
H2O-10-14	35	15	7	1	5	43	0.0038
H2O-10-20	35	15	7	1	5	43	0.0041
H2O-10-16	34	14	6	1	6	41	0.0042
H2O-10-25	35	15	7	1	5	43	0.0043
H2O-10-17	34	14	6	1	6	41	0.0044
H2O-10-21	34	14	6	1	6	41	0.0049
H2O-10-t24	35	15	7	1	6	43	0.0053
H2O-10-27	34	14	6	1	6	41	0.0054
H2O-10-E18	35	15	8	2	6	45	0.0058
H2O-10-t26	34	14	5	0	6	39	0.0059
H2O-10-E15	35	15	7	1	6	43	0.0062
H2O-10-E8	35	15	7	1	7	43	0.0065
H2O-10-E1	35	15	7	1	6	43	0.0070
H2O-10-29	34	14	5	0	6	39	0.0072
H2O-10-28	34	14	6	1	6	41	0.0072
H2O-10-E16	35	15	7	1	6	43	0.0082
H2O-10-t9	36	16	8	1	6	45	0.0088
H2O-10-E7	35	15	7	1	7	43	0.0089
H2O-10-t12	35	15	7	1	5	43	0.0096
H2O-10-E17	34	14	6	1	6	41	0.0099
H2O-10-t25	34	14	5	0	6	39	0.0118
H2O-10-t10	36(1)	15	8	1	5	45	0.0122
H2O-10-t15	34	14	6	1	6	41	0.0137
H2O-10-t7	35	15	7	1	6	43	0.0148
H2O-10-t17	34	14	5	0	6	39	0.0165
H2O-10-t27	36	16	7	0	6	43	0.0169
H2O-10-t23	37(2)	15	9	1	5	47	0.0170
H2O-10-t16	35	15	6	0	8	41	0.0182
H2O-10-t13	36(1)	15	8	1	7	45	0.0193
H2O-10-t28	33	13	4	0	8	37	0.0205
H2O-10-t18	33	13	4	0	7	37	0.0208